Immune-Competent 3D Bioengineered Colons for Functional Interrogation of Neuroinflammation-Induced Colonic Dysmotility

Claudia A. Collier[1], Aelita Salikhova[1], Shrinarayanee Rengarajan[1], Anvitha Tharakesh[1], Shanthi Srinivasan[2], and Shreya A. Raghavan[1]*

[1]Department of Biomedical Engineering, Texas A&M University
[2]Department of Medicine, Division of Digestive Diseases, Emory University

**Corresponding author:*
Department of Biomedical Engineering at Texas A&M University
3120 TAMU
College Station, TX, 77843, United States
E-mail: sraghavan@tamu.edu

ABSTRACT
Functional gastrointestinal disorders (FGIDs) affect ~40% of the global population and are frequently characterized by colonic dysmotility. Symptomatic manifestations of colonic dysmotility significantly reduce quality of life in inflammatory bowel disease (IBD), diabetes, and Gulf War Illness (GWI). Current in vitro models lack the integration of functional physiology with immune and neuronal complexity required to establish causal links between neuroinflammation and dysmotility. Here, an immune-competent bioengineered colon is introduced that integrates multiple cell types of the external colonic wall, along with functional readouts of motility. Within bioengineered colons, exposure to pyridostigmine bromide (PB), a toxicant associated with GWI, drove interferon-gamma mediated neuroinflammation. Contractile motility dysfunction occurred in PB-exposed bioengineered colons due to neural progenitor depletion, and impaired neuronal regeneration. In contrast, tumor necrosis factor-α (TNF-α), a cytokine central to IBD, induced NF-κB driven inflammation and smooth muscle remodeling, permitting partial neuronal recovery but sustaining dysmotility. The bioengineered colon model offered high fidelity in replicating diverse modes of enteric neuroinflammation. Ultimately, the platform offers a physiologically relevant avenue to interrogate neuroimmune crosstalk, dissect mechanisms of colonic dysmotility, and evaluate regenerative and therapeutic strategies for gastrointestinal pathologies.

INTRODUCTION

Functional gastrointestinal disorders (FGIDs) are a significant global health burden[1], affecting an estimated 40% of people globally[2]. Our understanding of its pathogenesis, and consequently, our ability to design targeted therapeutics to curtail it lag due to inadequately functional immune competent model systems. At the heart of FGIDs is altered colonic motility (colonic dysmotility). Symptomatic presentations of colonic dysmotility in FGIDs include chronic constipation or diarrhea, recurrent abdominal pain, and bloating. While these symptoms may appear minor individually, their chronic occurrence substantially impairs quality of life. FGIDs frequently coexist with or are exacerbated by other diseases. For example, approximately 25% of inflammatory bowel disease (IBD) patients experience colonic dysmotility[3]; diabetics have enteric neuropathy that also result in colonic dysmotility[4]. Additionally, toxic exposure-linked Gulf War Illness[5, 6] also manifests as colonic dysmotility. These facts underscore the significant global health burden of FGIDs and the critical need to understand their pathogenesis, especially the pervasive symptom of colonic dysmotility that contributes to poor quality of life and psychological distress.

The colon is extensively innervated by a dense neural network and is also a highly immune-competent organ[7]. Consequently, neuro-immune interactions in the gut are tightly regulated in homeostasis, infection, and inflammation[8, 9]. While these interactions are well-studied in mucosal barrier function[10], their role in colonic motility and FGIDs is still evolving[11]. Recent research has highlighted nuances in neuro-immune crosstalk, including the specific types of immune cells (T cells, macrophages, mast cells, etc.) and the types of neurons (sensory, motor, etc.) involved, which lead to diverse effects on colonic physiology[9, 12,13]. Particularly relevant to colonic motility and FGIDs is the regenerative interaction between macrophages and enteric nerves in the external muscle layers of the colon, away from the inner mucosa. This interaction is noteworthy because these external colonic layers regulate colonic motility. Consequently, dysregulated neuro-immune interactions here lead to colonic dysmotility, the primary dysfunction in FGIDs.

The turnover and regeneration of enteric neural circuitry and therefore motility rely on tissue-resident enteric neuronal progenitor cells. Tolerogenic macrophages help regeneration by clearing neuronal debris[14]. When inflammation disrupts this homeostatic neuro-immune interaction, the consequences can be profound: activated pro-inflammatory macrophages release cytokines that impair neuronal regeneration and smooth muscle contraction[15, 16], thereby affecting colonic motility. For example, our research with mouse models of Gulf War Illness demonstrated that toxic exposures reprogrammed macrophages and induced enteric neuronal progenitor cell apoptosis, leading to chronically altered colonic motility and FGID[17, 18]. Similar disruptions in neuroplasticity and altered colonic motility are routinely reported in mouse models of inflammatory bowel disease and FGIDs, often accompanied by increased pro-inflammatory cytokines[11, 13, 19, 20]. Collectively, the presence of altered neuroplasticity, increased pro-inflammatory cytokines and altered colonic motility supports a model in which macrophages, smooth muscle cells of the colon, and enteric neurons interact to contribute to the symptoms of colonic dysmotility[19, 21, 22].

Despite these insights, establishing causative mechanisms linking enteric neuro-inflammation to colonic motility remains challenging, largely due to the complexity scale in current experimental models. While mouse models excel at linking functional physiology to histological observations, they are tedious to interrogate molecular mechanisms. Herein, bioengineering and in vitro modeling offer a fantastic opportunity for tight variable control and mechanistic studies[23, 24]. However, many in vitro gut models fall short of mimicking the cellular complexity or structural organization required to integrate neuro-immune interactions with gut motility as a functional readout. Colonic organoids have been previously used to investigate immune signaling in inflammatory bowel disease[25], and macrophage-nerve interactions in FGID[26]. Despite their cellular complexity, organoids lack the spatial organization required to translate neuro-immune interactions into functional colonic motility[27]. The absence of functional readouts (spontaneous and evoked contractions in response to exogenous stimuli) limits their ability to capture how neuroinflammation drives colonic motility (and dysmotility). As a result, there is a pressing need for bioengineered culture systems that combine mechanistic accessibility with physiological relevance, enabling direct links between cellular dysfunction and tissue-level functional outcomes.

Here, we address this need by introducing an immune-competent 3D bioengineered colon model. This model controllably integrates key cell types of the colonic wall that regulate colonic motility. These cell types include smooth muscle cells, macrophages, and an enteric neural circuit derived from enteric neuronal progenitor cells. This platform structurally mimics the outer colon layer and enables real-time assessment of tissue contractility under defined neuroinflammatory conditions. In this study, we demonstrate the mechanistic capabilities of the bioengineered colon by examining the effects of distinct neuroinflammatory exposures—namely pyridostigmine bromide (PB - a toxic exposure linked to neuroinflammation in GWI[5, 17, 18]) and tumor necrosis factor alpha (TNF-α – a cytokine observed in many FGIDs[28, 29]). We show that bioengineered colons can discern how different neuroinflammatory stimuli alter nerve-macrophage interactions and the dynamics of neuronal progenitor cell-driven regeneration. Importantly, our model integrates these inflammatory events into functional colonic motility as a consequence of altered nerve-macrophage interaction, which is the central manifestation of FGIDs. Beyond its relevance to specific disease models, this system serves as a foundational versatile platform for probing neuroimmune mechanisms, facilitate the development of regenerative therapeutics, and modeling complex gastrointestinal pathologies characterized by chronic inflammation and impaired motility.

RESULTS AND DISCUSSION

Assembly of a 3D colon incorporating neural, smooth muscle, and immune lineages

Colonic motility arises from the muscularis externa of the colon, the outer layers that comprise smooth muscle cells, an integrated neuronal network and tissue-resident macrophages. To study functional consequences of enteric neuro-inflammation on colonic motility, we bioengineered the colonic muscularis externa. The bioengineered platform combined three key cell types within a collagen hydrogel: (i) immortalized colonic smooth muscle cells (icSMCs) as the smooth muscle component that generates the forces relevant to colonic motility; (ii) immortalized enteric neuronal progenitor cells (IM-FENs) that differentiate within the bioengineered construct to form mature neuronal networks; and (iii) immortalized macrophages (iBMDMs) to add immune competency. **Figure 1A** outlines the sequential cell seeding process into the collagen hydrogel, and subsequent self-assembly into concentric layered structures. Bioengineered colons matured over 3-7 days, enabling integrated neuro-immune structures and concentrically aligned smooth muscle architecture (**Figure 1B**). Compaction of the collagen hydrogel also occurred during the self-assembly process (>75% compaction over 3 days; **Figure 1C**).

Spatial and cellular maturation and organization within the bioengineered colons was confirmed via whole mount immunofluorescence (**Figure 1D**). By day 5, α-SMA$^+$ smooth muscle cells were concentrically aligned, similar to the structural organization of smooth muscle cells in the colon[30]. Differentiated neurons derived from neuronal progenitor cells robustly expressed βIII-tubulin$^+$, organized in reticular network-like structures similar to their organization within the myenteric plexus of the colon[31, 32]. Differentiated neuronal subtypes were further identified via stains specific to the synthesis of neurotransmitters, namely choline acetyltransferase (ChAT) and nitric oxide synthase (Nos1)[33]. Interestingly, our stains also demonstrated that bioengineered colons retained a population of neuronal progenitor cells in their progenitor state, evidenced by Ngfr-p75$^+$ staining, similar to tissue resident adult enteric neuronal stem cells present in the human and mouse colons[34, 35]. Macrophage presence was additionally verified by F4/80$^+$ expression interspersed within the bioengineered structure.

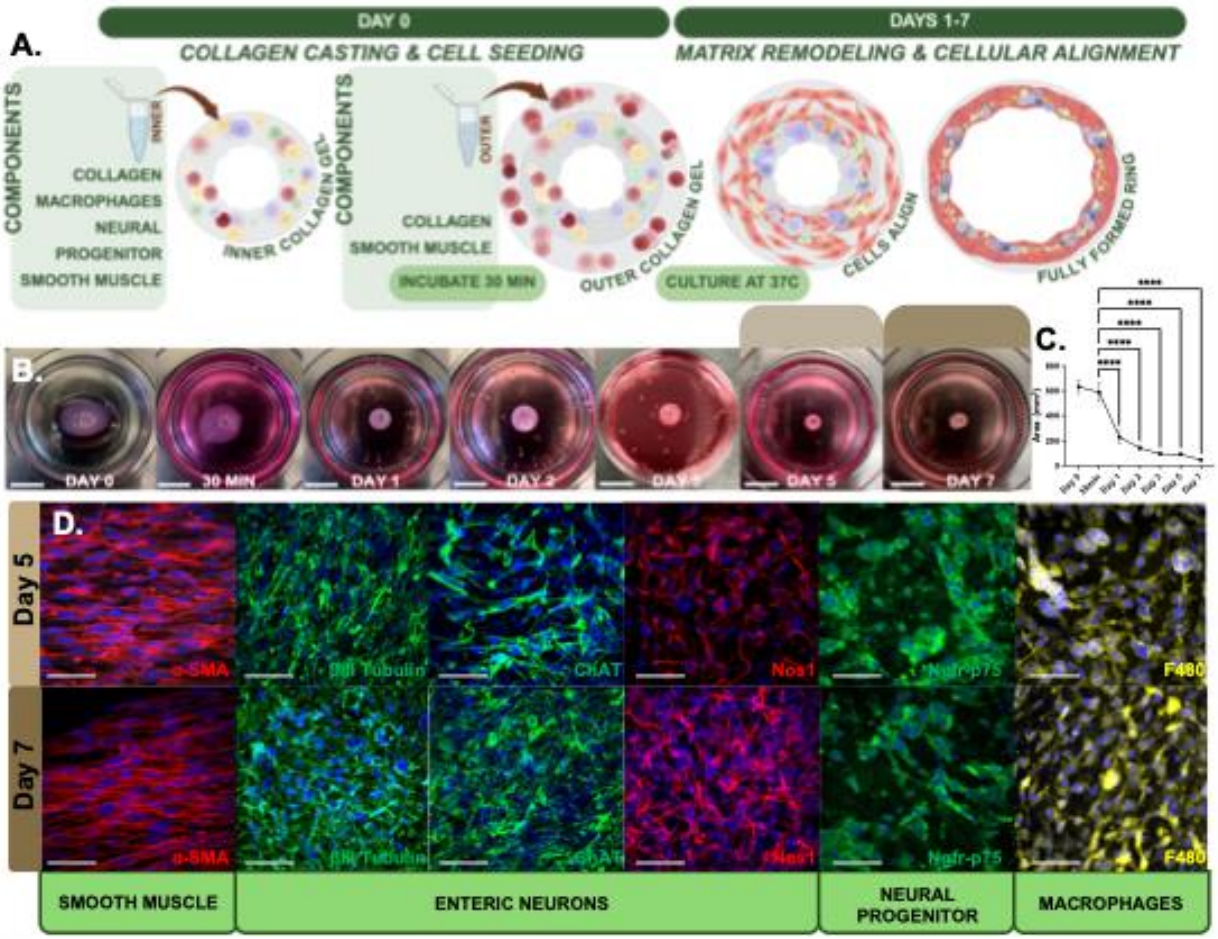

Figure 1. *Multicellular 3D bioengineered colon assembloid integrating smooth muscle, neural, and macrophage immune cells.* A) Schematic of the sequential collagen casting and cell seeding procedure. Layer 1 contains immortalized murine bone marrow-derived macrophages (iBMDM), immortalized murine fetal enteric neural progenitor cells (IM-FEN), and immortalized murine colonic smooth muscle cells (icSMC). These cells were embedded in an inner collagen gel, followed by a second collagen layer with icSMCs alone (outer collagen gel). Constructs were cultured for 7 days at 37°C to self-assemble into a ring-like structure with a defined hollow lumen. B) Representative photographs of bioengineered colons during layer-by-layer assembly, and every day from days 1-7. A central post defining the hollow luminal space is still visualized in these photographs, with the bioengineered circular colon around it. Scale bar = 15 mm (C) Quantification of bioengineered colon area over time with progressive compaction. ****$p<0.0001$, ordinary one-way ANOVA, $n>14$. (D) Wholemount immunofluorescence staining at days 5 and 7 demonstrating cellular markers: α-SMA (α-smooth muscle actin), βIII-tubulin (neuronal tubulin), ChAT (choline acetyltransferase), and Nos1 (neuronal nitric oxide synthase), Ngfr-p75 (receptor for the neural growth factor p75 labeling neural progenitor cells), F4/80 (pan-macrophage marker). Scale bar = 20 μm.

Bioengineered colons have distinct gene expression changes to stimulated neuro-inflammation

We next assessed the transcriptional consequences of inflammatory exposure in the bioengineered colon rings. We stimulated enteric neuro-inflammation using two different methods commonly associated with functional gastrointestinal disorders. The first stimulant was Pyridostigmine bromide (PB), a toxic exposure associated with Gulf War Illness. Our previous work has extensively shown that PB exposure potently induces enteric neuro-inflammation disrupting macrophage-nerve crosstalk in the colon[17, 18], resulting in severe colonic motility disruption. The second stimulant we used in this study was Tumor Necrosis Factor-alpha (TNF-α), central to enteric neuro-inflammation in inflammatory bowel diseases like Crohn's Disease[20], where colonic motility is similarly disrupted. **Figure 2A** displays a timeline for when inflammatory stimuli are added to bioengineered colons. PB or TNF-α stimulation occurred for 24hrs, following which an immediate response to inflammation was assessed (acute). Once inflammatory stimulants were removed, bioengineered colons were allowed to recover for 3 additional days, and a recovery from inflammation was assessed (chronic). All comparisons were made to untreated control bioengineered rings that were time-matched in culture.

PB-induced gene expression changes in bioengineered colons mirror those observed in Gulf War Illness mouse colons

Acute PB exposure significantly increased the gene expression of *Il6* (**3.68-fold**), with a subsequent drop to 2.62-fold chronically, indicating mild but incomplete recovery (**Figure 2B**). The elevated low-grade inflammation in bioengineered colons was in line with observations from mouse models of persistent enteric neuro-inflammation in Gulf War Illness[18]. Markers of reparative macrophages, *Mrc1* and *Ch3l3*, were acutely downregulated, with a partial restoration following recovery.

Acute PB exposure also resulted in a reduction of neuronal gene expression compared to untreated bioengineered colons (**Figure 2C**). Specifically, *Tubb3* (**0.85-fold; ****p<0.0001**), *Chat* (**0.68-fold; ****p<0.0001**), and *Nos1* (**0.73-fold; ****p<0.0001**) were all significantly decreased, indicating impaired neuronal programming. Interestingly, upon recovery, *Chat* expression trended towards significant upregulation (**2.97-fold; ****p<0.0001**). These findings in bioengineered colons also mimicked studies in Gulf War Illness mouse models, where one-time PB exposure chronically destroyed enteric neuronal integrity and altered neuronal subtype balance[18]. Neuronal recovery, despite subtype imbalance, was supported by increased gene expression of *Ngfr-p75* and *Sox2* (**Figure 2D**), in line with adult enteric neo-neurogenesis following inflammatory insult[36, 37], captured within bioengineered colons. Interestingly, PB exposure did not alter the gene expression of smooth muscle markers (**Figure 2E)**, also in line with our previous observations in mouse models[18].

TNF-α–induced gene expression changes are distinctly different compared to PB-induced changes in bioengineered colons

Bioengineered colons exposed acutely to TNF-α exhibited strong pro-inflammatory activation (**Figure 2F**), with significant upregulation of *Il6* (1.94-fold; ****p<0.01**). Reparative macrophage markers, *Mrc1* and *Ch3l3,* were reduced (**0.32-** and **0.44-fold**,

***p<0.001**) compared to control, with no evident recovery in gene expression levels. This is unsurprising, because TNF-α is a potent inflammatory mediator in macrophages, including in inflammatory bowel disease[20].

Neuronal damage and mild recovery were observed in bioengineered rings with TNF-α treatment, with acute downregulation of *Tubb3* and *Nos1,* but not *Chat* (**Figure 2G**). Markers of neuronal stemness were more broadly suppressed with TNF-α treatment, compared to PB, both acutely and chronically despite recovery. *Sox2* expression partially recovered to 0.89-fold (****p<0.0001)** but remained significantly lower than control (***p<0.05; Figure 2H**). *Ngfr-p75* slightly increased to 0.78-fold (****p<0.01**), while *Nes* declined further to 0.52-fold (****p<0.0001**) compared to acute rings, demonstrating complex and marker-specific neural stem cell regulation over chronic TNF-α induced inflammation.

Acute TNF-α exposure induced pronounced upregulation of smooth muscle contractile genes *Acta2* (**2.27-fold; ****p<0.0001**), *Cald1* (**1.75-fold; *p<0.05**), and *Tagln* (**1.19-fold; ns),** compared to control rings (**Figure 2I**)**.** In line with observations from experimental mouse models of inflammatory bowel disease, TNF-α exposure significantly alters expression of thin filament contractile elements within smooth muscle like Caldesmon (*Cald1*) and Smoothelin (*Tagln),* that ultimately result in impaired colonic contractility and motility[38, 39]. Bioengineered colons capture this important nuance, where TNF-α treatment resulted in changes in the smooth muscle compartment within the bioengineered colon, while PB did not.

Unbiased transcriptomics captures distinctions in PB and TNF-α induced enteric neuro-inflammation within bioengineered colons

In order to capture the differences in bioengineered colon response to both acute and chronic PB or TNF-α stimulation, we performed three-dimensional principal component analysis (3D PCA) on bulk RNA-seq data from treated and untreated bioengineered colons. The acute 3D PCA plot (**Figure 2J**) illustrates distinct clustering of the three groups along principal components 1, 2, and 3, which collectively explain 68.9% of the total variance (PC1 = 52.7%, PC2 = 9.8%, PC3 = 6.4%). Samples from PB- and TNF-α treated groups separate clearly from controls, demonstrating transcriptomic alterations in response to inflammatory challenge. These transcriptional distinctions persisted into the chronic phase, as shown in the chronic PCA plot (**Figure 2K**), where the three groups again clustered separately, with total variance explained reaching 70.4% (PC1 = 41.8%, PC2 = 16.8%, PC3 = 11.8%). This continued separation suggests lasting and distinct transcriptional remodeling despite removal of the initial stimulus.

The upregulated gene sets (**Figure 2L**) revealed both overlapping and distinct genes: a core subset of 91 genes was commonly upregulated by both PB and TNF-α, likely indicative of shared inflammatory pathways. Additionally, TNF-α uniquely upregulated 344 genes, while PB uniquely upregulated 133 genes, reflecting stimulus-specific transcriptional programs. Similarly, the downregulated gene sets (**Figure 2M**) revealed an overlap of 8 genes, with TNF-α driving broader suppression of 169 unique genes

compared to PB's 9 unique genes. After recovery, chronic exposure led to even more divergent transcriptional responses. A total of 408 genes were uniquely upregulated by PB, and 680 by TNF-α, with 66 genes commonly upregulated between the two treatments (**Figure 2N**). Similarly, 366 genes were uniquely downregulated by PB, 227 by TNF-α, and 53 genes were shared (**Figure 2O**).

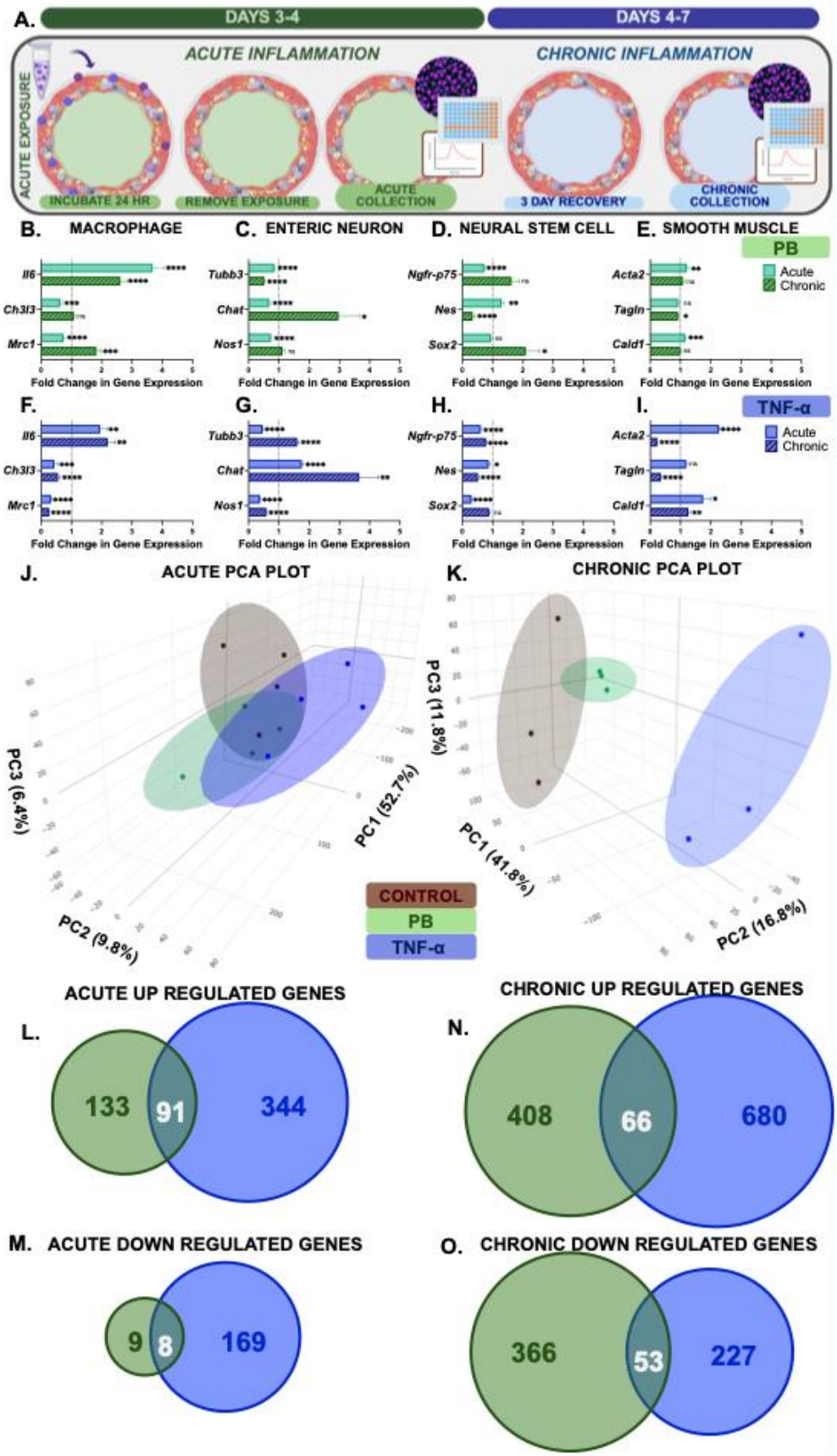
A.
DAYS 3-4
DAYS 4-7
ACUTE INFLAMMATION
CHRONIC INFLAMMATION
ACUTE EXPOSURE
INCUBATE 24 HR
REMOVE EXPOSURE
ACUTE COLLECTION
3 DAY RECOVERY
CHRONIC COLLECTION
B. MACROPHAGE
C. ENTERIC NEURON
D. NEURAL STEM CELL
E. SMOOTH MUSCLE
PB
Acute
Chronic
Il6
Ch3l3
Mrc1
Tubb3
Chat
Nos1
Ngfr-p75
Nes
Sox2
Acta2
Tagln
Cald1
Fold Change in Gene Expression
F.
G.
H.
I.
TNF-α
J. ACUTE PCA PLOT
K. CHRONIC PCA PLOT
PC1 (52.7%)
PC2 (9.8%)
PC3 (6.4%)
PC1 (41.8%)
PC2 (16.8%)
PC3 (11.8%)
CONTROL
PB
TNF-α
ACUTE UP REGULATED GENES
L.
133
91
344
CHRONIC UP REGULATED GENES
N.
408
66
680
M. ACUTE DOWN REGULATED GENES
9
8
169
O. CHRONIC DOWN REGULATED GENES
366
53
227

Figure 2. *Transcriptomic changes in bioengineered colons induced by exposure to Pyridostigmine bromide (PB) or Tumor necrosis factor (TNF-α).* A) Experimental timeline illustrating acute (24hr exposure) and chronic (3-day recovery post 24hr acute exposure) treatment conditions. (B–E) Gene expression analysis in PB-exposed bioengineered colons for macrophage (*Il6, Ch3l3, Mrc1*) (B), enteric neuron (*Tubb3, Chat, Nos1*) (C), neural stem cells (*Ngfr-p75, Nes, Sox2*) (D), and smooth muscle (*Acta2, Tagln, Cald1*) (E) markers, comparing acute and chronic conditions to untreated control. (F–I) Corresponding gene expression changes in TNF-α exposed rings for macrophage (F), enteric neuron (G), neural stem cell (H), and smooth muscle (I) markers. The dotted line at 1 represents the normalized level of gene expression for time-matched control colons. Data are presented as mean ± SEM. ****$p<0.0001$, ***$p<0.001$, **$p<0.01$, *$p<0.05$, 'ns' = not significant, one sample t-test, $n>3$. (J, K) Three-dimensional principal component analysis (PCA) of bulk RNA-seq showing clustering of control (brown), PB-treated (green), and TNF-α treated (blue) bioengineered colon samples under acute (J) and chronic (K) conditions. Each dot represents an individual biological replicate. % values indicate the proportion of total variance within each principal component. (L, M) Venn diagram comparing overlapping of significantly upregulated (L) and downregulated (M) genes between acute PB and TNF-α exposure. (N, O) Venn diagram comparing overlapping of significantly upregulated (N) and downregulated (O) genes between chronic PB and TNF-α exposure.

Gene Ontology and biological process analyses reveal shared and distinct mechanisms of PB and TNF-α induced inflammation and impaired neurogenesis

Noting that PB and TNF-α exposure generated distinct inflammatory signatures within bioengineered colons (differentially regulated genes also visualized as volcano plots in **Supplementary Figure 1A, B**), we explored unbiased RNA-Seq analysis to further determine distinctions. **Supplementary Figure 1** also demonstrates distinct genes that drive unique but strong immunologic signatures upon PB and TNF-α exposure, with distinctions between the two exposures broken down further in **Supplementary Figure 2**. The involvement of shared and distinct gene signatures was further highlighted via unbiased gene ontology and biological process (GO; BP) enrichment analyses (**Figure 3A-D**). Both stimuli (PB and TNF-α) resulted in positive regulation and activation of innate immune response within the bioengineered colon. Within the colonic muscularis externa, macrophages are key regulators of immune response to inflammation and stress, resulting in changes in colonic motility and neuronal health[16]. Transcriptomic changes confirmed that macrophages included within the bioengineered colon were able to respond to inflammatory stimuli like PB or TNF-α, the functional consequences of which we explore later in the study.

Despite the seeming similarities of inflammation responses initiated by PB and TNF-α, a deeper investigation of enriched gene sets revealed distinct molecular mechanisms underlying the exposures (**Figure 3A-D, Supplementary Figure 3**). For each identified pathway, a z-score was calculated based on the proportion of significant genes within the pathway.

The toxic exposure-based stimulant PB resulted in pronounced interferon-gamma based inflammatory responses in both acute and chronic settings (**Figure 3A-B; Supplementary Figure 3A,B)**, in line with many observations in Gulf War veterans that have higher serum levels of interferon-gamma[40, 41]. In fact, interferon-gamma based neuro-inflammation is documented to drive many neurological disorders central to Gulf War Illness, priming the innate immune system to sustain neuro-inflammation chronically[42].

In contrast to PB exposure, acute TNF-α exposure drove inflammation via NF-κB signaling, with strong enrichment of cellular response to interleukin-1 (**Figure 3C-D**; **Supplementary Figure 3C**). TNF-α and interleukin-1 are elevated in functional gastrointestinal disorders and inflammatory bowel disease[43], and their mechanisms of inflammation including in the colon are very well documented[44]. However, chronic TNF-α exposure strongly enriched chemotaxis (**Supplementary Figure 3D**), where this persistent immune cell recruitment contributes to tissue remodeling and fibrosis[45].

Chronic PB and TNF-α exposures also induced distinct transcriptional signatures, identified using the ChEA3 database (**Figure 3E-H**), with regulatory transcription factor-gene interaction maps in **Supplementary Figure 4**. Corroborating the theme that PB exposure drove an interferon-driven regulatory network, acute exposure and chronic recovery were dominated by transcription factors: *Stat1*[46], *Irf9*[47] and *Batf2*[48] (**Figure 3E,F**). In acute PB-exposed bioengineered colons, *Stat1* stood out as a central regulator linking multiple target genes such as *Cxcl10*[49], *Cxcl9*[50], and *Ciita*[51] (**Supplementary Figure 4A**) to coordinate inflammation. In chronic PB-exposed rings, networks reorganized around *Cd36*, *Ciita*, and *Stat1*, integrating transcriptional input from *Ppara*, *Nfe2l2*, and *Csf1* to link immune activity with metabolic and stress-adaptive pathways[52] (**Supplementary Figure 4B**).

In contrast, TNF-α exposure revealed prominent involvement of *Plscr1*[53, 54], *Relb*[55], and *Etv7*, indicating differential transcriptional control linked to inflammatory signaling pathways (**Figure 3G**). However, chronic TNF-α exposure produced an entirely distinct set of transcription factors (*Tcf21, Msx1*, and *Foxf1*[56]) that are more commonly linked to developmental and matrix remodeling (**Figure 3H**). Acute TNF-α exposure revealed a more complex regulatory landscape with *Nos2*, *Ccl5*, and *Cxcl10* as major hub of genes controlled by a broad array of transcription factors including *Batf2*, *Stat3*, *Rel*, *Irf1*, and *Jun* (**Supplementary Figure 4C**). Similarly, chronic TNF-α exposure preserved core inflammatory drivers such as *Nos2* and *Nfkb1* but expanded to include matrix remodeling and fibrotic regulators (*Mmp9, Mmp3*[57], *Smad3*[58], *Serpine2*[59]), suggesting persistence of inflammatory signaling alongside induction of tissue remodeling programs (**Supplementary Figure 4D**).

Overall, unbiased transcriptomic analysis revealed that bioengineered colons were capable of distinctly responding to inflammatory stimuli, initiated either by PB exposure or by TNF-α exposure. Importantly, even after removal of the initial insult (chronic conditions), each exposure sustained divergent signatures during recovery: PB-driven responses remained centered on interferon-gamma mediated neuroinflammation and

impaired neurogenesis, while TNF-α shifted toward extracellular matrix remodeling and fibrotic pathways. The impact of these stimuli in many ways mirrored published pathways implicated in individuals with Gulf War Illness (instigated by PB exposure), or inflammatory bowel disease (driven by TNF-α).

Figure 3. *Transcriptomic profiling and biological process enrichment following exposure to PB and TNF-α in bioengineered colon rings.* (A, B) Top unbiased Gene Ontology (GO) Biological Processes (BP) significantly enriched in acute PB (A) and chronic PB (B) treated rings. Bars represent the –log10 adjusted p-value for each GO term. (C, D) Top unbiased GO BP significantly enriched in acute TNF-α (C) and chronic TNF-α (D) treated rings. (E, F) Top predicted transcription factors associated with upregulated gene expression changes following acute PB (E) and chronic PB (F) treatments, ranked by integrated scoring. (G, H) Top predicted transcription factors associated with upregulated gene expression changes following acute TNF-α (G) and chronic TNF-α (H) treatments, ranked by integrated scoring.

Cytokine profiling reveals distinct protein levels changes in bioengineered colons under neuro-inflammatory stimuli

Secreted cytokines are key orchestrators of tissue damage downstream of inflammatory initiation. Given the prevalent, yet distinct, inflammatory gene signatures in bioengineered colons with PB and TNF-α exposure, we next investigated changes in a panel of secreted cytokines that amplify inflammation[60-64], mediate neural repair[65, 66] or are associated with tissue damage within the colonic muscularis externa[67]. PB and TNF-α treatment demonstrated partially distinct profiles (**Figure 4**).

Single PB exposure results in chronic low-grade neuro-inflammation and pathological tissue remodeling

Acute exposure to PB triggered a robust pro-inflammatory response in bioengineered colons, characterized by elevated CCL2, IL-1β, and IL-6 (*****p<0.001; Figure 4A; 'Acute'**) and decreased IL-10 (******p<0.0001**). This mirrors neuro-inflammatory profiles reported in the muscularis externa of GWI-affected colons[17, 18].

Following removal of PB, the inflammatory environment in bioengineered colons evolved (noted as 'Chronic' in **Figure 4**): TIMP-1 and CCL11 levels increased (******p<0.0001**), reflecting pathological tissue remodeling commonly seen within the inflamed colon[68, 69]. Low-grade, unresolved inflammation persisted through elevated IL-6 and IL-1β, along with low IL-10 levels, similar to GWI[70]. Additionally, persistent elevation of β-NGF (****p<0.01**) was indicative of neuroinflammation driven altered neuronal plasticity[71]. Together, these findings showed that PB exposure induced a chronic low-grade inflammatory state in the macrophage-immune competent bioengineered colon, replicating features observed in the pathogenesis of GWI-associated colonic dysfunction.

TNF-α induced secretome partially reflects inflammation resolution with time

Acute TNF-α exposure prompted pro-inflammatory cytokine secretion (IL-1β, IL-6) in bioengineered colon tissues (**Figure 4B; 'Acute'**). Interestingly, TNF-α (but not PB) immediately increased TIMP-1, a sign of acute pathological tissue remodeling. Following the removal of TNF-α, bioengineered colons progressed partially towards recovery (**Figure 4B; 'Chronic'**), with plummeting levels of IL-1β, IL-6 and TIMP-1. Mild signatures of neuro-inflammation were still persistent, including a potential recovery, with elevated CCL11 and β-NGF. Bioengineered colons were able to mirror time-dependent

inflammatory cytokine landscapes and remodeling processes similar to that observed in the colon, that contribute to motility dysfunction within the muscularis externa[72, 73].

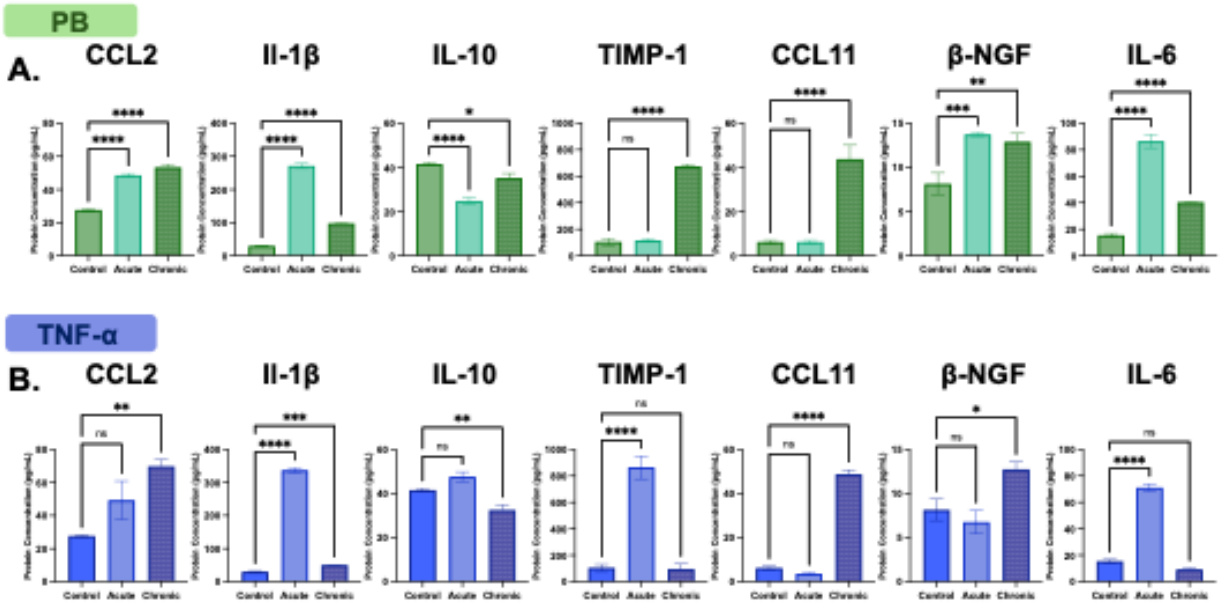

Figure 4. *Cytokine profiling of bioengineered colons following exposure to PB and TNF-α.* (A, B) Multiplex Luminex quantification of inflammatory and regulatory cytokines from bioengineered colon rings under control, acute (24-hr exposure), and chronic (3-day recovery post-exposure) conditions. Analyzed cytokines include: CCL2 (monocyte chemoattractant protein-1), IL-1β (interleukin-1 beta), IL-10 (interleukin-10), TIMP-1 (tissue inhibitor of metalloproteinases-1), CCL11 (eotaxin), β-NGF (beta-nerve growth factor), and IL-6 (interleukin-6). A) Cytokine levels following PB treatment in bioengineered colons. B) Cytokine levels following TNF-α treatment in bioengineered colons. Data are presented as mean ± SEM. ****$p<0.0001$, ***$p<0.001$, **$p<0.01$, *$p<0.05$, 'ns' = not significant; ordinary one-way ANOVA; $n>3$.

Wholemount immunostaining reveals structural changes in bioengineered colons with neuro-inflammatory stimulation

Next, we used whole mount immunostaining to visualize structural changes that resulted from secreted factors and gene expression associated with neuro-inflammation, tissue remodeling, and neural plasticity. As the likely responder and orchestrater of inflammation, we first assayed macrophage numbers and phenotypes within the bioengineered colons. Overall neuronal network integrity was assessed using βIII-tubulin, with cholinergic subtypes visualized via ChAT (choline acetyltransferase), and inhibitory nitrergic subtypes using Nos1 (neuronal nitric oxide synthase). The continued presence of neuronal progenitor cells was also assayed, since these progenitor cells contribute to neuronal repair. Lastly, the effectors of motility, the smooth muscle cells were identified for their arrangement using α-smooth muscle actin (**Figure 5**). Changes were compared between control untreated and PB or TNF-α stimulated bioengineered colons.

PB exposure drives sustained inflammation with impaired neural regeneration

Inflammatory Cd40$^+$ macrophages significantly increased with PB-treatment, rising 15% acutely and staying elevated by 37% in chronic conditions compared to time-matched untreated controls (***p<0.05; Figure 5A-C**). No changes were observed in reparative Ym1$^+$ macrophages, consistent with its associated gene expression of *Ch3l3* (**Figure 2B**) and relatively stable levels of IL-10 (**Figure 4A**).

Acute and sustained inflammation lead to neuronal degeneration[17, 74, 75]. Structural damage of the neuronal network was evident with visual changes in βIII-tubulin organization (84% reduction with PB, compared to untreated controls; **Figure 5A-C**). Cholinergic and nitrergic neuronal subtypes were also reduced (79% and 73% respectively; ***p<0.05; Figure 5B, C**). Acute cholinergic nerve loss is unsurprising following PB treatment, since PB reversibly inhibits acetylcholine esterase, thereby directly targeting cholinergic nerves[76]. Sustained loss of neuronal integrity despite recovery ('Chronic' in **Figure 5B-C**) reflects a compromised neuronal repair system[77]. Consistent with this notion, PB treatment reduced neuronal progenitor cells by 87% (Ngfr-75; ***p<0.05; Figure 5A-C**) with no recovery, contributing to the disarrayed neuronal network.

Smooth muscle alignment and structural integrity largely remained unchanged, with only minor fluctuations (9% increase acutely, 3% decrease chronically; **Figure 5A-C**), in line with gene expression data (**Figure 2E**). This stability suggested that smooth muscle structural integrity was preserved despite neuroimmune disruption.

TNF-α exposure drives distinct neuronal changes along with reactive smooth muscle hypertrophy

Similar to PB-exposure, TNF-α also increased inflammatory Cd40$^+$ macrophages in bioengineered colons (23% acutely and 37% chronically compared to untreated controls; ***p<0.05; Figure 5D-F**). Unchanging reparative Ym1 dynamics continued to suggest an impaired resolution of inflammation and transition to reparative phenotypes, in the timeframes the bioengineered colons were examined.

TNF-α exposure also contributed to acute disintegration of neural network integrity (69% loss in βIII-tubulin fluorescence, ***p<0.05, Figure 5D-F**). While cholinergic ChAT$^+$ neurons were not affected with TNF-α like PB, a severe loss of nitrergic Nos1$^+$ neurons occurred. The loss in nitrergic nerves is in line with therapeutic evidence that anti-TNF monoclonal antibodies aid in robust nitrergic neuronal recovery in experimental IBD models[78]. Interestingly, following recovery to TNF-α exposure, neuronal network integrity and ChAT$^+$ neurons were fully restored (**'Chronic' TNF-α, Figure 5E**). This mild neurotrophic effect of TNF-α on enteric neurons, especially in co-culture systems where smooth muscle cells are present has been observed previously[79], and replicated within bioengineered colons.

As expected, α-SMA expression increased acutely by 67% (****p<0.01**), consistent with reactive smooth muscle hypertrophy observed in IBD[80, 81]. This contrasts with the stable α-SMA levels seen following PB exposure. During recovery, α-SMA expression returned to baseline, indicating a resolution of the hypertrophic response over time.

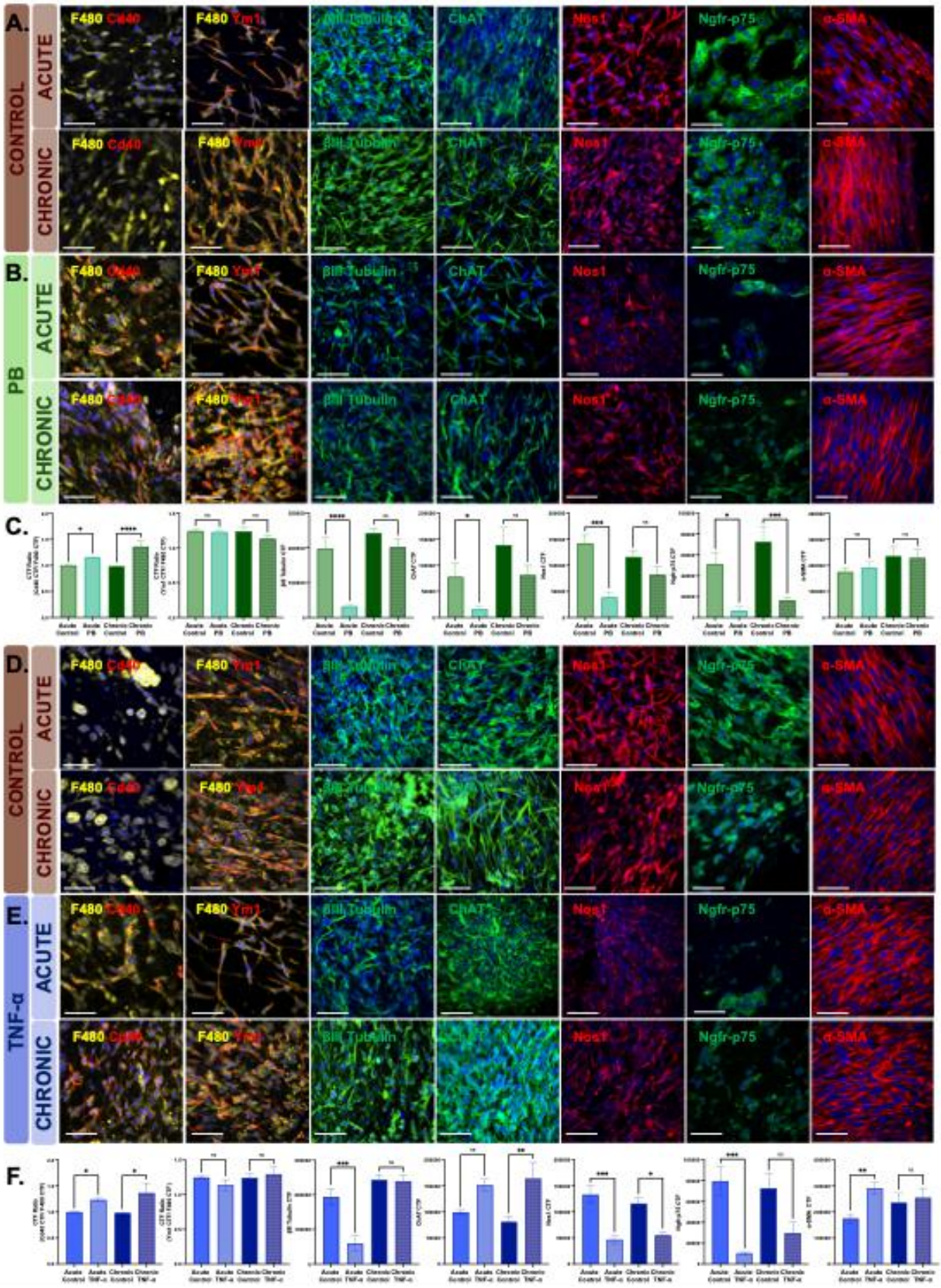
A.
CONTROL
ACUTE
CHRONIC
F480 Cd40
F480 Ym1
βIII Tubulin
ChAT
Nos1
Ngfr-p75
α-SMA
B.
PB
ACUTE
CHRONIC
C.
D.
CONTROL
ACUTE
CHRONIC
E.
TNF-α
ACUTE
CHRONIC
F.

Figure 5. *Wholemount immunostaining in bioengineered colons as untreated controls or following PB or TNF-α exposure.* (A–C) Representative immunofluorescence images of control (A) and PB-exposed (B) bioengineered colons at acute (24hrs following stimulation) and chronic (3 days following stimulation and recovery) timepoints. Scale bar = 20 μm. (C) Quantification of macrophage phenotypes (F4/80, yellow; Cd40, red; Ym1, red), neuronal subtypes (βIII-tubulin, ChAT, Nos1- all green), neural progenitors (Ngfr-p75, green), and smooth muscle (α-SMA, red) in control and PB-treated bioengineered colons under acute (24-hr exposure) and chronic (3-day recovery) conditions. (D–F) Representative immunofluorescence images of control untreated (D) and TNF-α (E) treated bioengineered colons at acute and chronic timepoints. Scale bar = 20 μm. (F) Quantification of control and TNF-α treated rings at acute and chronic time-points. Data are presented as mean ± SEM. ****$p<0.0001$, ***$p<0.001$, **$p<0.01$, *$p<0.05$, 'ns' = not significant; ordinary one-way ANOVA; $n>5$.

Inflammatory exposures impair colonic motility in a 3D bioengineered colon model

Altered colonic motility is a hallmark of both GWI[82] and IBD[83, 84], contributing significantly to functional gastrointestinal disorders and reduced quality of life[85-87]. Coordinated contractile function is a complex interplay of homeostatic macrophage immune activation, structural integrity of smooth muscle cells, intact neuronal architecture and balanced neuronal subtypes. In response to inflammatory stimuli in bioengineered colons, we observed pervasive changes in inflammatory macrophage activation (Cd40 enrichment in Figure 5; cytokine secretome in Figure 4; genotype in Figures 2-3), the structure of smooth muscle arrangement (like those observed in Figure 5E), and neuronal damage and imbalance in neurochemical coding (seen as imbalanced ChAT/Nos neurons in Figure 5). We hypothesized that these changes will alter colonic motility in PB or TNF-α exposed colons compared to control, untreated colons. To this end, we assessed contractile behavior in bioengineered colons using a force transducer-based organ bath system[17, 18, 88]. Bioengineered colons were stabilized in organ baths, and contractions were recorded following exogenous stimuli designed to interrogate both neuronal and smooth muscle contributions. Representative contractility traces from control and inflamed rings (PB- and TNF-α exposed) are shown in **Figure 6**, with time on the X-axis and force amplitude relative to baseline on the Y-axis.

Inflammation causes persistent impairment of colonic contractile function mediated by cholinergic neuronal activity

Contractile function was assessed by exogenous addition of acetylcholine (ACh; timing indicated by arrows in **Figure 6**). To isolate neuronal functionality in addition to the direct effect of ACh on smooth muscle cells, bioengineered colons were pre-treated with a nerve blocker, tetrodotoxin (TTX; green dotted traces in **Figure 6**). Control untreated bioengineered colons displayed robust ACh-induced contractions with an average peak force of 132.0 ± 0.8 μN (black trace, **Figure 6A, C**). Pretreatment with TTX significantly reduced contractile amplitude by 67% (green dotted trace, ******$p<0.0001$; Figure 6B**), confirming the presence of a functional neuronal component capable of mediating contractions within bioengineered colons[88].

Both PB and TNF-α treatment reduced ACh-induced contractile magnitude (53% lower in PB; 44% lower in TNF-α; ******p<0.0001, ***p<0.001; Figure 6B, C**). Interestingly, acute structural loss of cholinergic nerves with PB treatment (but not TNF-α) manifested functionally as muted sensitivity to TTX pre-treatment (only 23% sensitive in PB-exposed bioengineered colons, compared to 67% sensitivity in untreated controls and 64% sensitivity in TNF-α treated colons). Following removal of PB and recovery, contractile dysfunction persisted in chronic PB-treated bioengineered colons (**Figure 6D-F**), similar to loss of contractility in GWI colons[17]. Only partial recovery of contractility was observed in chronic TNF-α treated colons (***p<0.001; ****p<0.01**; **Figure 6E, F**), despite a recovery of structural neuronal integrity. The broader colonic dysmotility is further supported by immunostaining and gene expression data, where an imbalance in excitatory and inhibitory neuronal populations is evident, which can impair coordinated motility[18, 89, 90]. Especially in the TNF-α treated colons, a further contributing factor to diminished contractility is the reactive changes in smooth muscle that can alter muscle responsiveness, limiting contractile efficiency[91, 92].

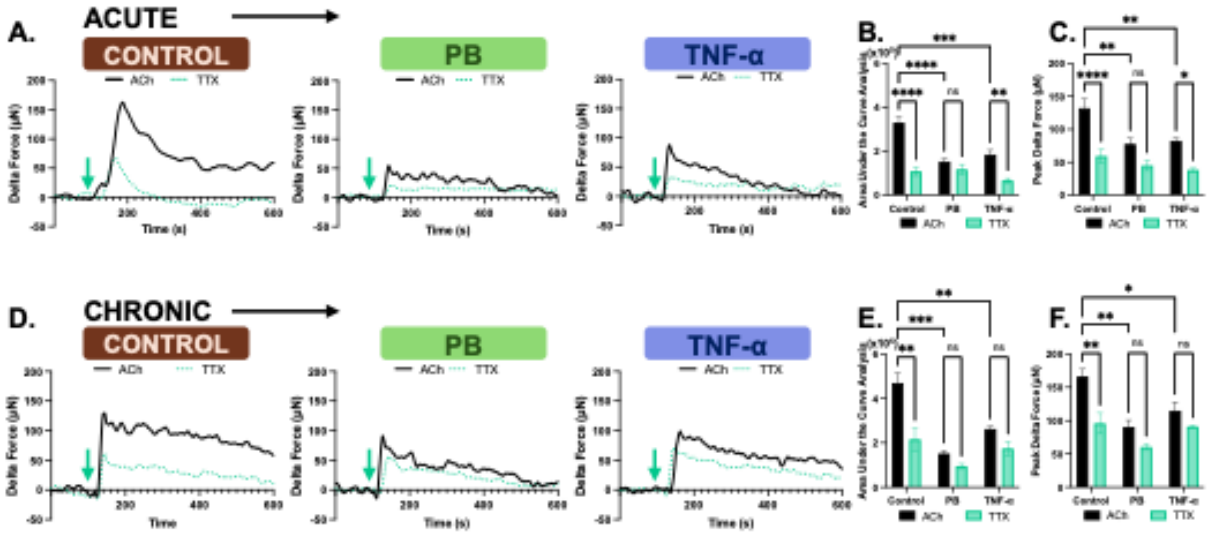

Figure 6. *Inflammatory exposures impair neuronally mediated contractility in 3D bioengineered colons.* Bioengineered colons were mounted in a force transducer-fitted organ bath, and contractile force was measured in response to exogenous addition of acetylcholine (ACh). ACh addition is indicated by the blue arrow, after the establishment of a stable baseline of force (arbitrarily set to zero). (A) Representative traces in response to 1 μM ACh (black traces) stimulation in control untreated or acute exposure to PB-, or TNF-α. Neuronal contributions were isolated by pre-treatment with 1 μM tetrodotoxin (TTX, blue dotted lines. (B) Quantification of contractile output as area under the curve for various treatment conditions under acute exposure. Data are presented as mean ± SEM. ****p<0.0001, ***p<0.001, **p<0.01, 'ns' = not significant; two-way ANOVA; n>5. (C) Quantification of contractile output as peak magnitude of force generated following ACh stimulation in acute conditions. Data are presented as mean ± SEM. ****p<0.0001, **p<0.01, *p<0.05, 'ns' = not significant; two-way ANOVA; n>5. (D) Representative traces in response to ACh stimulation in chronic bioengineered colons, maintained as untreated controls or 3 days recovered from PB or TNF-α treatment. (E) Quantification of contractile

output as area under the curve for various treatment conditions under chronic exposure. Data are presented as mean ± SEM. ***p<0.001, **p<0.01, 'ns' = not significant; two-way ANOVA; n>3. (F) Quantification of contractile output as peak magnitude of force generated following ACh stimulation in chronic conditions. Data are presented as mean ± SEM. **p<0.01, *p<0.05, 'ns' = not significant; two-way ANOVA; n>3.

Macrophages resolve inflammation in a time-dependent manner after acute inflammatory stimulus

While our 3D bioengineered colon model captures the complex interactions between inflammation, neural populations, and motility, the presence of multiple interacting cell types and extracellular matrix components makes it difficult to determine which specific cells are responsible for releasing inflammatory mediators and driving the sustained neural damage and dysfunction. To disentangle the direct effects of inflammatory stimuli, such as PB and TNF-α, we employed a simplified macrophage monoculture system.

We cultured iBMDMs to assess temporal dynamics of macrophage activation and resolution following acute inflammatory insults. Cells were treated with either PB or TNF-α for 24 hours, followed by either immediate analysis (acute) or recovery in fresh media for 3 or 5 days (chronic) (**Figure 7A**).

PB exposure induces robust but reversible inflammatory macrophage activation
Acute PB exposure significantly upregulated pro-inflammatory gene expression of *Il6* by 14-fold, confirming activation of a classical inflammatory response (******p<0.0001; Figure 7B**). Upon removal of PB, *Il6* gene expression decreased in a time-dependent manner declining substantially over 7 days, with a steady and concurrent upregulation of *Ch3l3* and *Mrc1*. In parallel, inflammatory Cd40 expression peaked with acute PB exposure (2-fold increase; ****p<0.0001; **Figure 7C, D**) with a gradual decline over 7 days. Secreted cytokine patterns also mirrored the acute inflammation (increases in CCL2, IL-1β, CCL11 and IL-6) with an active decline towards baseline over time (**Figure 7E**). Together, these results demonstrated that PB induced inflammation in macrophages was robust, but reversible, with a shift towards resolution of inflammation in the absence of other cell types amplifying tissue damage.

TNF-α induces a transient pro-inflammatory macrophage response followed by reparative activation during recovery
Acute TNF-α exposure significantly upregulated *Il6* gene expression by 3.8-fold (******p<0.0001; Figure 7F**), confirming induction of a pro-inflammatory macrophage activation. Similar to PB exposure, *Il6* expression declined progressively to near-baseline levels (1.5-fold; ******p<0.0001**), with increased gene expression of reparative markers, *Mrc1* and *Ch3l3* (******p<0.0001; Figure 7F**). Macrophages also transiently increased Cd40 expression, with a gradual decline following removal of TNF- α and recovery (**Figure 7G, H**). Secreted cytokines also matched these activation patterns (**Figure 7I**). This temporal pattern parallels the response to PB, highlighting the ability of macrophages to consistently resolve inflammation across different inflammatory contexts.

This resolution observed in macrophage monocultures contrasts with the persistent inflammation seen within 3D bioengineered colons, where complex multicellular interactions and extracellular matrix components likely sustain pro-inflammatory signaling and impede full recovery. Thus, while macrophages have an intrinsic capacity to resolve inflammation after PB exposure in vitro, the 3D microenvironment introduces additional regulatory factors that complicate resolution, highlighting the importance of studying inflammation in physiologically relevant contexts.

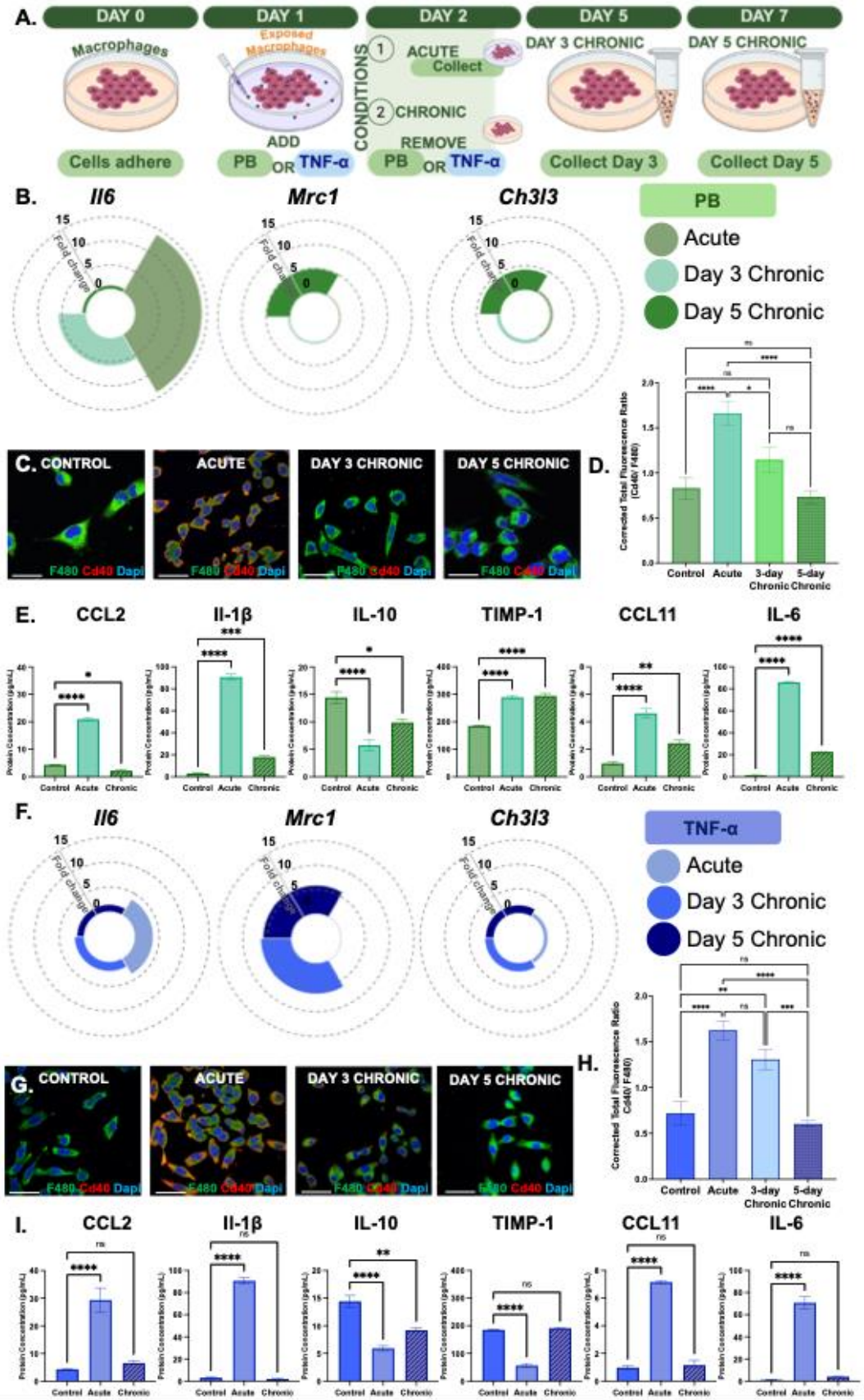
A.
DAY 0
DAY 1
DAY 2
DAY 5
DAY 7
Macrophages
Exposed Macrophages
CONDITIONS
1 ACUTE
Collect
2 CHRONIC
DAY 3 CHRONIC
DAY 5 CHRONIC
Cells adhere
ADD
PB OR TNF-α
REMOVE
PB OR TNF-α
Collect Day 3
Collect Day 5
B.
Il6
Mrc1
Ch3l3
Fold change
PB
Acute
Day 3 Chronic
Day 5 Chronic
C. CONTROL
ACUTE
DAY 3 CHRONIC
DAY 5 CHRONIC
F480 Cd40 Dapi
D.
Corrected Total Fluorescence Ratio (Cd40/ F480)
Control
Acute
3-day Chronic
5-day Chronic
E.
CCL2
Il-1β
IL-10
TIMP-1
CCL11
IL-6
Protein Concentration (pg/mL)
F.
TNF-α
Acute
Day 3 Chronic
Day 5 Chronic
G.
H.
I.

Figure 7. *Time-Dependent Resolution of Macrophage Activation and Secretory Profiles Following Acute PB and TNF-α Exposure* (A) Schematic outlining the experimental timeline for macrophage stimulation and recovery. Immortalized bone marrow-derived macrophages (iBMDMs) were treated with 100 μM PB or 100 ng/mL TNF-α for 24 hours (acute), followed by either immediate sample collection or a recovery period in fresh media for 3 or 5 days (chronic). (B) Circular bar plots showing average gene expression fold changes of macrophage markers (*Il6*, *Mrc1*, *Ch3l3*) following acute and chronic PB exposure. (C) Representative immunofluorescence images of macrophages stained for F4/80 (green), Cd40 (red), and DAPI (blue) under control, acute, and chronic PB conditions. Scale bar = 15μm. (D) Quantification of Cd40 expression in control and PB-treated macrophages. Data are presented as mean ± SEM. ****p<0.0001, *p<0.05, 'ns' = not significant; ordinary one-way ANOVA; n>5. (E) Cytokine levels following PB treatment in macrophages. Data are presented as mean ± SEM. ****p<0.0001, ***p<0.001, **p<0.01, *p<0.05; ordinary one-way ANOVA; n>3. (F) Average gene expression fold changes of macrophage markers (*Il6, Mrc1, Ch3l3*) following TNF-α treatment. (G) Representative immunofluorescence images of macrophages stained for F4/80 (green), Cd40 (red), and DAPI (blue) under control, acute, and chronic TNF-α conditions. Scale bar = 15μm. (H) Quantification of Cd40 expression in control and TNF-α treated macrophages. Data are presented as mean ± SEM. ****p<0.0001, ***p<0.001, **p<0.01, 'ns' = not significant; ordinary one-way ANOVA; n>5. (E) Cytokine levels following TNF-α treatment in macrophages. Data are presented as mean ± SEM. ****p<0.0001, **p<0.01, 'ns' = not significant; ordinary one-way ANOVA; n>3.

Inflammatory secretome from PB-exposed macrophages disrupts neural stem cell maintenance and impairs neuronal differentiation

Within bioengineered colons, PB exposure (but not TNF-α) persistently damaged neuronal structural integrity (**Figure 5**), resulting in functional dysmotility (**Figure 6**). We hypothesized that such persistent dysmotility occurs due to impaired regenerative and repair of enteric neural circuitry within the bioengineered colon, initiated by Ngfr-75 enteric neuronal progenitor cells. This hypothesis was partially based on our previous observations in mouse models of PB-exposure, where inflammatory Cd40 macrophages lay in close proximity to $p75^+$ enteric neuronal progenitor cells within the colonic myenteric plexus[18]. Here, we sought to establish direct causal evidence of PB-related inflammation impeding enteric neural stem progenitor mediated regeneration of neurons.

We employed a monoculture model of immortalized p75+ enteric neuronal progenitor cells (IM-FENs)[93], which possess the ability to differentiate into motor neuronal subtypes[88]. First, we directly exposed IM-FENs to PB to assess their intrinsic sensitivity to inflammatory insult (**Supplementary Figure 5**). While PB treatment induced some changes in proliferation and differentiation, the overall effects of PB on differentiation capability were modest. Therefore, we hypothesized that any impairment in enteric neuronal progenitor differentiation might be macrophage immune-mediated, rather than direct toxic exposure.

To test this hypothesis, we next applied conditioned media collected from PB-treated macrophages (PB-CM; iBMDMs) to IM-FEN cultures (**Figure 8A**). IM-FENs were chronically exposed to conditioned medium, to simulate ongoing enteric neuro-inflammation.

PB-CM reduces enteric neuronal progenitor proliferation and depletes progenitor identity

Ki67 immunostaining revealed a marked reduction in proliferative IM-FENs following exposure to PB-CM (**Figure 8B**), compared to untreated controls. Quantitative analysis showed a 31% decrease in Ki67^{+} cells at day 5, and 28% at day 7 in PB-CM treated cultures relative to untreated controls (****p<0.01; Figure 8C**), suggesting a potential impairment in self-renewal ability. This reduced proliferative capacity was accompanied by an 82% decline in Ngfr-p75^{+} cells (a marker of stem-like identity) (******p<0.0001; Figure 8D**), indicating that prolonged exposure to inflammatory CM severely compromises neural progenitor maintenance. The gating strategy for all flow analysis is provided in **Supplementary Figure 6.** Gene expression analysis supported these findings, showing significant downregulation of neural stem cell markers *Ngfr-p75 (***0.36-fold**)*, Nestin (***0.94-fold**), and *Sox2 (***0.38-fold***)* in PB-CM treated IM-FENs (******p<0.0001; Figure 8E**), consistent with loss of stem-like phenotype. Overall, sustained exposure to inflammatory macrophage-conditioned media significantly compromises both the proliferative capacity and neural progenitor maintenance of IM-FENs.

Inflammatory PB-CM impairs neuronal differentiation of IM-FENs

Neural progenitor cells are essential for maintaining productive neuroplasticity in response to inflammation. To understand how inflammation affects this regenerative potential in neuronal progenitor cells, we evaluated neuronal differentiation in the presence of PB-CM. When stimulated to differentiate with exogenously added factors, neuronal progenitor cells demonstrated an impaired ability to differentiate with reduction in βIII-tubulin, ChAT, and Nos1 in PB-CM treated cultures compared to controls (**Figure 8F, G**). This loss of neuronal markers was supported by gene expression analysis, which revealed 49% and 52% reductions in *Chat* and *Nos1* expression (*****p<0.001; Figure 8H**). These results reveal a marked impairment in neurogenesis under PB-mediated inflammation, characterized by loss of neuronal identity and differentiation capacity.

These findings support our hypothesis that PB-induced, macrophage-mediated inflammation impairs enteric neural repair and contributes to dysmotility. In our PB-exposed bioengineered colon model, we observed sustained inflammation, and activation of cell death pathways, as evidenced by transcriptomic profiling (**Figures 3**) and elevated levels of inflammatory cytokines (**Figure 4**), alongside major neuronal losses and inflammatory macrophage accumulation (**Figure 5**). Collectively, this suggests that PB exposure initiates a strong macrophage-driven inflammatory response that persists beyond the initial insult, leading to long-term disruption of neurogenesis and neural circuit integrity. This chronic neuroinflammation (despite PB removal) likely explains the loss of functional motility observed in our PB-exposed bioengineered colon model.

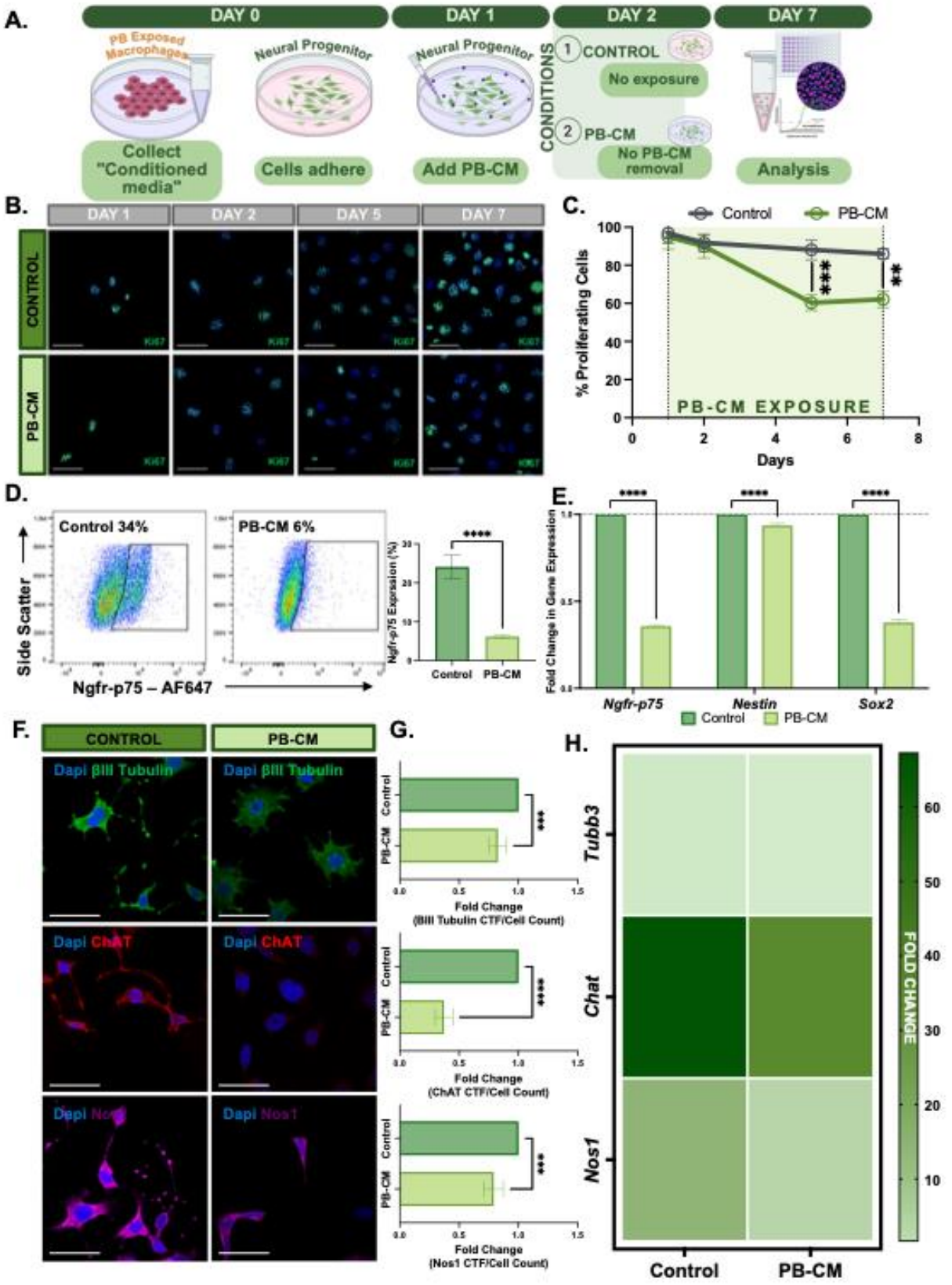
A.
DAY 0
DAY 1
DAY 2
DAY 7
PB Exposed Macrophages
Neural Progenitor
Neural Progenitor
CONDITIONS
1 CONTROL
No exposure
2 PB-CM
No PB-CM removal
Collect "Conditioned media"
Cells adhere
Add PB-CM
Analysis
B.
DAY 1
DAY 2
DAY 5
DAY 7
CONTROL
PB-CM
C.
Control
PB-CM
% Proliferating Cells
PB-CM EXPOSURE
Days
D.
Control 34%
PB-CM 6%
Side Scatter
Ngfr-p75 – AF647
Ngfr-p75 Expression (%)
Control
PB-CM
E.
Fold Change in Gene Expression
Ngfr-p75
Nestin
Sox2
Control
PB-CM
F.
CONTROL
PB-CM
Dapi βIII Tubulin
Dapi ChAT
Dapi Nos1
G.
Fold Change (βIII Tubulin CTF/Cell Count)
Fold Change (ChAT CTF/Cell Count)
Fold Change (Nos1 CTF/Cell Count)
H.
Tubb3
Chat
Nos1
FOLD CHANGE
Control
PB-CM

Figure 8. *Inflammatory secretome from PB-exposed macrophages disrupts IM-FEN proliferation and neurogenic potential.* (A) Schematic of experimental timeline for treating IM-FENs with conditioned media collected from PB-exposed macrophages (PB-CM). (B) Representative immunofluorescence images showing Ki67 (green), a marker of proliferating cells, in untreated and PB-CM treated IM-FEN cultures at the indicated timepoints. Nuclei are counterstained with DAPI (blue). Scale bars = 15 µm. (C) Quantification of Ki67^{+} proliferating cells over 7 days. Data are presented as mean ± SEM. ****$p<0.0001$, **$p<0.01$, two-way ANOVA; $n>5$. (D) Flow cytometry analysis of neural progenitor marker Ngfr-p75 expression in control and PB-CM treated IM-FENs. Data are presented as mean ± SEM. ****$p<0.0001$, unpaired t-test; $n>9$. (E) Relative gene expression of neural stem markers *(Ngfr-p75*, *Nestin*, *Sox2)* in PB-CM treated IM-FENs, normalized to untreated controls (dotted line = 1). Data are presented as mean ± SEM. ****$p<0.0001$, 'ns' = not significant; two-way ANOVA; $n>4$. (F, G) Untreated or PB-CM treated IM-FENs were differentiated into several neuronal subtypes. (F) Representative immunofluorescence images showing expression of neuronal markers: βIII-tubulin (green), ChAT (red), and Nos1 (magenta) in control and PB-CM treated differentiated IM-FENs. Nuclei are counterstained with DAPI (blue). Scale bars = 20 µm. (G) Quantification of differentiated neuronal populations expressing βIII-tubulin, ChAT, and Nos1. Data are presented as mean ± SEM. ****$p<0.0001$, ***$p<0.001$; unpaired t-test; $n>5$. (H) Heatmap displaying relative gene expression fold changes of *Tubb3*, *Chat*, and *Nos1* in untreated and PB-CM treated differentiated IM-FENs, normalized to undifferentiated controls.

CONCLUSIONS

Our findings position macrophage-driven neuroinflammation as a central mechanism in the pathogenesis of functional gastrointestinal disorders. Leveraging a multicellular, immune-competent 3D bioengineered colon model with direct contractility readouts, this study demonstrates that distinct inflammatory stimuli engage unique neuroimmune responses: toxic exposure via pyridostigmine bromide drove interferon-gamma mediated chronic inflammation, whereas TNF-α activated NF-κB dependent remodeling. Both inflammatory stimuli converged on neuronal loss, impaired neurogenic repair, and persistent colonic motility dysfunction. Crucially, inflammatory macrophage secretomes directly suppressed enteric neural progenitor proliferation and differentiation, defining a mechanistic axis for failed neuronal regeneration. By capturing these stimulus-specific and chronic signatures, the model mirrors the lasting and heterogeneous course of dysmotility observed across Gulf War Illness and Inflammatory Bowel Disease. Beyond recapitulation, this platform integrated immune, neural, and muscular compartments, enabling mechanistic interrogation, future therapeutic screening, and development of regenerative strategies. These advances set the stage for employing patient-derived cells for personalized disease modeling and drug discovery. While further validation in primary human tissues and in vivo contexts is warranted, our model bridges the current gap between simplified in vitro assays and complex animal studies, laying a foundation for precision therapies targeting neuroimmune drivers of gastrointestinal disease.

ACKNOWLEDGMENTS
The authors acknowledge the assistance of the Integrated Microscopy and Imaging Laboratory at the Texas A&M College of Medicine (RRID:SCR_021637). Figures were partially created with BioRender.com.

AUTHOR CONTRIBUTIONS
Conceptualization: C.A.C.; S.A.R.; Data curation: C.A.C.; Formal analysis: C.A.C., S.A.R.; Funding acquisition: S.A.R.; Investigation: C.A.C., A.S.; Methodology: C.A.C., S.A.R.; Project administration: C.A.C., S.A.R.; Resources: S.A.R., S.S.; Software: C.A.C.; Supervision: C.A.C., S.A.R.; Validation: C.A.C., S.A.R.; Visualization: C.A.C., A.S., A.V., S.A.R.; Writing – original draft: C.A.C., S.A.R. ; Writing – review & editing: C.A.C., S.A.R, S.S.

FUNDING
This work was supported by the Department of Defense Gulf War Illness Research Program W81XWH-21-0477 (S.A.R.), Department of Defense Toxic Exposures Research Program HT9425-24-1-0998 (S.A.R.), Texas A&M University Avilés-Johnson Graduate Fellowship Program (C.A.C.), the National Defense Science and Engineering Graduate (NDSEG) Fellowship Program (C.A.C.) through the Army Research Office, and NIH R01 DK080684 (S.S.).

DATA AVAILABILITY STATEMENT
Raw data supporting the findings in this study will be deposited in Zenodo with a DOI prior to publication. RNA-Seq datasets will be deposited on the GEO database, and all associated code will be deposited on the Raghavan Lab Github (github.com/SRaghavanLab).

METHODS
Materials and reagents
All tissue culture media, and supplements were purchased from ThermoFisher Scientific (Waltham, MA, USA), unless otherwise specified. Growth factors and proteins were purchased from Peprotech (Cranbury, NJ, USA). All conjugated antibodies were purchased from Santa Cruz (Dallas, TX, USA), Cell Signaling Technology (Danvers, MA, USA), or Abcam (Cambridge, MA, USA), unless specified otherwise. Pyridostigmine bromide, Acetycholine (ACh), Tetrodotoxin (TTX) were purchased from Sigma Aldrich (St. Louis, MO, USA).

Cell lines and culture
Isolation And Culture of Immortalized Colonic Smooth Muscle Cells (icSMCs)
Primary murine colonic smooth muscle cells were isolated from adult mouse colon via sharp dissection, enzymatic digestion, and filtration as previously described[17]. Briefly, dissected colonic tissue was minced and digested in type I collagenase, then filtered through a 40 µm mesh and plated in complete Dulbecco's Modified Eagle Medium (DMEM) supplemented with 10% fetal bovine serum + 1% penicillin and streptomycin. After initial expansion, cells were transduced with EF1α-SV40 large T antigen (SV40T)

lentiviral particles (GeneCopoeia, puromycin-selectable; Rockville, MD, USA) to establish a stable immortalized smooth muscle cell line (icSMC). Successfully transduced cells were selected using puromycin and maintained at 37°C with media changes every 48 hours.

Culture Of Immortalized Bone Marrow Derived Macrophages

Immortalized bone marrow derived macrophages[94] (iBMDMs) were a gift from Dr. Philip West's laboratory at Jackson Labs, Bar Harbor ME. Cells were maintained in complete DMEM supplemented with 10% fetal bovine serum + 1% antibiotic-antimycotic at 37°C with 5% CO_2.

Culture Of Immortalized Fetal Enteric Neural Cells (IM-FENs):

The immortalized murine fetal enteric neuron (IM-FEN) cell line used in this study was generated and characterized by the Srinivasan Laboratory at Emory University[93, 95].Briefly, IM-FENs were derived from E13 H-2Kb-tsA58 immortomouse embryos. Neural precursors were isolated using magnetic bead immunoselection targeting the low-affinity NGF receptor (Ngfr-p75). IM-FENs were maintained in a modified N2 medium supplemented with 10% fetal bovine serum, 10 ng/mL glial cell line-derived neurotrophic factor (GDNF), 20 U/mL recombinant mouse interferon-γ, and 1% penicillin/streptomycin. Cells were cultured at 33°C in a humidified incubator with 5% CO_2 to preserve their progenitor state. To induce neuronal differentiation, cells were transitioned to a 1:1 ratio of conditioned media collected from icSMCs and neurobasal-A medium supplemented with B-27 (serum-free), 2 mmol/L L-glutamine, 1% heat-inactivated fetal bovine serum, 1% penicillin/streptomycin, and 10 ng/mL GDNF. Cultures were maintained at 39°C and 5% CO_2 for up to 7 days to promote differentiation into mature enteric neurons.

Bioengineered colon ring formation

Bioengineered colonic rings were fabricated using a two-layer collagen hydrogel deposition technique within 35-mm tissue culture dishes fitted with a central silicone post (3-mm outer diameter; Sylgard® 184 Silicone Elastomer Kit, Denver, CO, USA) to define the lumen. The base layer consisted of a mixture containing 400,000 cells/mL IM-FENs, 1,500 cells/mL iBMDMs, and 200,000 cells/mL icSMCs suspended in 1 mg/mL collagen type I, rat tail (ibidi; Madison, WI, USA). The mixture was cast around the central post and allowed to gel at 37°C for 15 minutes. A second layer containing 600,000 cells/mL icSMCs in collagen was then overlaid and allowed to gel for an additional 30 minutes at 37°C. Following gelation, 2 mL of SMC media was added to each dish, and constructs were incubated at 37°C to promote alignment and matrix compaction. After 24 hours, media was supplemented with neuronal differentiation media for a final 1:1 ratio of icSMC media: neural differentiation media to support differentiation and network integration. Constructs were cultured for 3 days before adding inflammatory insults.

Inflammatory Stimulation of Bioengineered Colon Rings

Once bioengineered colon rings were established and fully formed (days 1- 3), they were maintained as untreated controls or exposed to 100μM PB or 100ng/mL TNF-α for 24 hours. To investigate acute effects of inflammatory exposure, inflammatory stimulus was removed after 24hrs and immediately collected for downstream analysis. To observe

chronic effects after a single one-time exposure, bioengineered rings were allowed to recover for an additional 3 days after removing inflammatory exposure, supplemented with fresh media.

Monoculture exposures of macrophages to inflammatory stimuli

For toxic insult, iBMDMs were seeded overnight in densities ranging from 3,000 – 8,000 cells/mL before adding 100μM PB or 100ng/mL TNF-α for 24 hours. iBMDMs were assessed at different time points: 'Acute' was collected immediately after 24 hours of exposure; 'Chronic' conditions were replaced with fresh growth media after the initial 24-hour exposure and allowed to recover for 3 and 5 days. Media was also collected from iBMDMs following acute exposure to PB, sterile filtered and termed as 'PB-conditioned media (PB-CM)'.

Conditioned Media Experiments and IM-FEN Cultures

IM-FENs were seeded at densities of 8,000 cells/mL overnight before adding 100μM PB for 24 hours (single one-time exposure) or PB-CM for the duration of the experiment. IM-FENs set to differentiate were seeded on fibronectin coated wells. Briefly, wells were coated with 50μg/mL of fibronectin (Sigma Aldrich; St. Louis, MO, USA) for 2 hours, rinsed with PBS and seeded with cells. Cultures first were placed in 33°C overnight before supplementing with neural differentiation media and toxic insult (either 100μM PB or PB-CM) and placed at 39°C with 5% CO_2.

RNA extraction and gene expression via q-PCR

RNA was extracted from cultured cells using a RNeasy extraction kit (Qiagen, Hilden, Germany). Bioengineered rings were first flash frozen in liquid nitrogen, minced in cold TRIzol™ LS Reagent (Invitrogen, Carlsbad, CA, USA) and extracted using the same kit following manufacture's protocol. RNA concentrations were measured using a Nanodrop 2000 (ThermoFisher Scientific, Carlsbad, CA, USA) spectrophotometer, transcribed to cDNA using the high-fidelity cDNA transcription kit (Life Technologies, Carlsbad, CA, USA), and q-PCR was carried out in the 96-well format using a QuantStudio (Applied Biosystems, Foster City, CA, USA). Gene expression differences were quantified using the 2ΔΔCT method, using *Gapdh* as the housekeeping control, and reported as fold changes compared to a control sample. qPCR experiments were run in triplicates with 5 independent samples. Primer sets used are detailed below (**Table 1**).

Table 1. List of primers used in RT-qPCR analysis of gene expression.

Mouse Primer	Gene Sequences
Gapdh	F: AGGTCGGTGTGAACGGATTTG
	R: GGGGTCGTTGATGGCAACA
Nos1	F: CCCAACGTCATTTCTGTCCGT
	R: TCTACCAGGGGCCGATCATT
Chat	F: GGCCATTGTGAAGCGGTTTG
	R: GCCAGGCGGTTGTTTAGATACA
Tubb3	F: CCCAGCGGCAACTATGTAGG
	R: CCAGACCGAACACTGTCCA
Ngfr-p75	F: TGCCGATGCTCCTATGGCTA

	R: CTGGGCACTCTTCACACACTG
Sox2	F: GCGGAGTGGAAACTTTTGTCC
	R: GGGAAGCGTGTACTTATCCTTCT
Nes	F: CCCACCTATGTCTGAGGCTC
	R: GGGCTAAGGAGGTTGGATCAT
Mrc1	F: CTCTGTTCAGCTATTGGACGC
	R: TGGCACTCCCAAACATAATTTGA
Ch3l3	F: CAG GTC TGG CAA TTC TTC TGA A
	R: GTC TTG CTC ATG TGT GTA AGT GA
Il6	F: TCT ATA CCA CTT CAC AAG TCG GA
	R: GAA TTG CCA TTG CAC AAC TCT TT
Cald1	F: AGA AGG AGT TTG ATC CGA CCA
	R: CAT TTT CGG CGG AGT CAT TTT G
Tagln	F: ACC AAA AAC GAT GGA AAC TAC CG
	R: GTG AAG TCC CTC TTA TGC TCC T
Acta2	F: GGC ACC ACT GAA CCC TAA GG
	R: ACA ATA CCA GTT GTA CGT CCA GA

Immunofluorescence methods

Cells were fixed with 4% Paraformaldehyde in PBS (Santa Cruz, Dallas, TX, USA) at room temperature for 20 minutes. Cells were then washed with 0.1M glycine for 5 minutes at room temperature, followed by permeabilizing and blocking (10% normal goat serum + 0.2% TritonX-100) for 45 minutes at room temperature. Cells were subsequently stained with fluorophore-conjugated antibodies (**Table 2**) and incubated overnight at 4°C. A nuclear counterstain (DAPI) was also included in the antibody incubation. Unbound antibody was washed with phosphate-buffered saline (PBS), and cells were mounted using Prolong Diamond anti-fade reagent (ThermoFisher Scientific (Waltham, MA)). Fluorescence was observed using an Olympus Fluoview FV3000 Confocal Laser Scanning Microscope (RRID:SCR_021637).

Wholemount Immunofluorescence

Bioengineered colonics were fixed in 4% paraformaldehyde for 30 minutes at room temperature, followed by three washes in phosphate-buffered saline (PBS). Colons were washed in 0.1M glycine for 20 minutes at room temperature followed by permeabilizing and blocking for 2 hours. Fluorophore-conjugated antibodies targeting lineage-specific markers (**Table 2**) were diluted in blocking buffer and incubated overnight at 4°C. Samples were then washed thoroughly before mounting. Mounted colons were imaged using Olympus Fluoview FV3000 Confocal Laser Scanning Microscope (RRID:SCR_021637). Each experimental condition was replicated across multiple biological samples ($n \geq 5$).

Table 2. List of antibodies used in immunohistochemistry.

Antibody	Conjugation	Manufacturer	Catalog #	RRID
F4/80	Alexa Fluor 488	Abcam	ab204266	AB_2943479
Ym1	PE	Abcam	ab211621	AB_3083045
Cd40	Alexa Fluor 647	Abcam	ab275158	AB_2839768

Ngfr-p75	Alexa Fluor 647	Santa Cruz Biotechnology	sc-271708	AB_10714958
βIII-Tubulin	Alexa Fluor 488	invitrogen	53-4510-82	AB_1107000
ChAT	FITC; Alexa Fluor 647	Santa Cruz Biotechnology	sc-55557	AB_2291743
Nos1	Alexa Fluor 647	Santa Cruz Biotechnology	sc-5302	AB_631879
SMα	Coralite 594	Proteintech	cl595-14395	AB_2889885
Ki67	Alexa Fluor 488	Cell signaling Technologies	11882S	AB_2797703

Quantification of Immunofluorescence

Immunofluorescence images of differentiated neurons stained for βIII-Tubulin, ChAT, and Nos1 were captured using consistent acquisition settings across all experimental conditions (control, PB, CM, and TNF-α). Quantitative analysis was performed using the corrected total fluorescence (CTF) method in FIJI/ImageJ from previously established protocols[17, 18, 96]. For each image, integrated density, area, and mean background fluorescence were measured for each ROI. CTF was calculated using the following formula:

CTF = Integrated Density − (Area of ROI × Mean Background Fluorescence)

To account for variations in cell number, CTF was divided by the number of nuclei (DAPI-positive cells) in each image, yielding an average CTF per cell. These CTF values were then normalized to the mean value from the control group to allow for relative comparison across conditions. Each experimental condition was replicated across multiple biological samples ($n \geq 5$).

To assess macrophage activation, iBMDMs were co-stained for F480 (pan-macrophage marker) and Cd40 (pro-inflammatory activation marker) and imaged using standardized acquisition settings across all experimental groups. Quantification was performed using the same CTF method in ImageJ. For each image, Cd40 CTF was divided by the corresponding F480 CTF to generate a normalized Cd40/F480 fluorescence ratio, representing the degree of pro-inflammatory polarization relative to total macrophage content. Each experimental condition was replicated across multiple biological samples ($n \geq 5$).

The primary antibody, Ki67 (Alexa Fluor 488) was used to mark active cell proliferation. $Ki67^+$ cells were identified by the presence of green fluorescence within DAPI (blue fluorescence) counterstained nuclei and were quantified manually using previously demonstrated protocols[97]. Analysis was performed to determine the number of actively proliferating cells (Ki67 antigen in the nuclei) versus the total cell number (number of nuclei) to determine the percentage of proliferating cells. Exposed cells were compared

to controls. Each experimental condition was replicated across multiple biological samples (n ≥ 5).

Functional testing of bioengineered colons

Physiological contractility of bioengineered colons were assessed using a custom-built organ bath system adapted from Collier et al.[17, 18]. Each ring was mounted by securing one end to a fixed post and the other to the arm of a force transducer (FT20, Harvard Apparatus). The organ bath was filled with DMEM buffered with 1 M HEPES and maintained at 37°C. The force transducer was calibrated, and baseline noise was recorded in both air and warm media prior to mounting bioengineered colonic tissues.

A 30% passive stretch was applied using a micromanipulator and maintained throughout the experiment to record isometric force. Rings were equilibrated under these conditions for 40–60 minutes. Baseline force post-equilibration was arbitrarily set to zero to allow for direct comparison of pharmacologically induced changes in contractility.

To assess neural responsiveness and muscle function, rings were treated with the following agents: Acetylcholine (ACh, 1 μM/mL) to induce cholinergic contraction; Tetrodotoxin (TTX, 1 μM/mL) to inhibit neuronal sodium channels and block neuronal activity.

Pharmacologic agents were added directly to the bath, and contractile responses were recorded. Force traces were analyzed for peak amplitude and area under the curve (AUC) to quantify physiological responses. Each experimental condition was replicated across multiple biological samples (n ≥ 5).

RNA isolation for RNA-sequencing

Bioengineered colons from control, PB, TNF-α were flash frozen using liquid nitrogen and then lysed and homogenized in TRIzol reagent (Invitrogen, Carlsbad, California). RNA was then extracted using a RNeasy extraction kit (Qiagen, Hilden, Germany). RNA concentrations were measured using a Nanodrop 2000 (ThermoFisher Scientific, Carlsbad, CA, USA) spectrophotometer. Library preparation with poly(A) selection and 150-bp paired-end sequencing on an Illumina HiSeq 2500 were performed by Azenta (South Plainfield, NJ, USA).

Computational analysis of RNA-seq data

Raw sequencing data in FASTQ format were generated by Azenta Life Sciences using an Illumina platform. Azenta performed initial quality assessment, adapter trimming, alignment, and gene count quantification. Specifically, adapter sequences and low-quality bases were trimmed using Trimmomatic v0.36, and trimmed reads were aligned to the *Mus musculus* GRCm38 reference genome (Ensembl) using STAR aligner v2.5.2b. Gene-level quantification was performed using featureCounts from the Subread package v1.5.2, generating a raw gene count matrix for each sample.

All subsequent computational and statistical analyses were conducted in-house using RStudio (2025.05.1+513) and R packages listed below. Differential gene expression

analysis (DGE) was performed using the DESeq2 package. Genes with p-value < 0.05 and absolute log2 fold change > 1.25 were defined as differentially expressed genes (DEGs).

Volcano plots were generated using ggplot2 and dplyr, and 3D principal component analysis (PCA) was performed using plotly and dplyr to visualize sample clustering based on transcriptomic profiles. Venn diagrams were used to compare the number of upregulated and downregulated DEGs across conditions relative to controls.

Gene ontology (GO) enrichment analysis was conducted using the EnRichGO, clusterProfiler, org.Mm.eg.db, AnnotationDbi, and tidyverse packages. Biological process (BP) terms were assessed for DEGs with log2FC > 1.25 and p-value < 0.05. In addition to the full GO output, a focused set of terms relevant to immune signaling, apoptosis, and neuroinflammation was selected for targeted enrichment: GO:0071347, GO:0019221, GO:0032755, GO:0032760, GO:0006935, GO:0006968, GO:0010942, GO:0034341, GO:0010977.

Transcription factor prediction was performed using the ChEA3 platform (https://amp.pharm.mssm.edu/ChEA3)[98], using the "TopRank" integrated library and inputting all upregulated DEGs for each condition. Network visualization was carried out using NetworkAnalyst (https://www.networkanalyst.ca)[99] by submitting the top five upregulated genes per condition to generate protein–protein interaction networks.

Luminex assay for cytokine release

Cell culture supernatants were collected from iBMDMs under control conditions or following treatment with PB or TNF-α, either acutely (24 hours) or after a 5-day recovery period post-exposure (chronic condition). Bioengineered colons were flash frozen with liquid nitrogen and collected in a RIPA+HALT solution. Supernatants were clarified by centrifugation at 500 × *g* for 5 minutes and stored at −80°C until analysis. Protein concentration was measured using a Pierce BCA assay (Thermo-Fisher). Cytokine levels were evaluated using bead-based multiplex immunoassays and done according to the manufacturer's protocol (R&D Systems, Minneapolis, MN). List of cytokines detailed in **Table 3.** Each experimental condition was replicated across multiple biological samples (n ≥ 3).

Table 3. List of cytokines used in bead-based multiplex immunoassay.

Cytokine	
C-C motif chemokine ligand 2	CCl2
Interleukin-1 beta	IL-1β
Interleukin-10	IL-10
Tissue Inhibitor of Metalloproteinases-1	TIMP-1
C-C motif chemokine ligand 11	CCL11
Beta-Nerve Growth Factor	β-NGF
Interleukin-6	IL-6

Flow analysis for Ngfr-p75$^+$ cells

IM-FENs were characterized using flow cytometry for Ngfr-p75 expression[100], by adapting previously used flow analysis protocols[17, 18]. Briefly, IM-FENs were collected and resuspended in a flow cytometry amenable buffer (PBS + 2% FCS) at a concentration of 200,000 cells/ml. Cells were incubated with a p75-AF647 antibody, with a matched isotype control. Cells were then processed through a flow cytometer (Attune NxT, Waltham, MA, USA). Flow cytometry analysis was completed with FlowJo (Ashland, OR). Polygon gates were drawn on isotype flow cytometry graphs to establish a background cut off gate at 0.5% (gating strategy is presented in **Supplementary Figure 6**). The same gate was applied to antibody-stained cells to establish a percent positive population. Each experimental condition was replicated across multiple biological samples (n ≥ 3).

REFERENCES

1. Sperber AD, Bangdiwala SI, Drossman DA, et al. Worldwide Prevalence and Burden of Functional Gastrointestinal Disorders, Results of Rome Foundation Global Study. Gastroenterology 2021;160:99-114.e3.
2. Fikree A, Byrne P. Management of functional gastrointestinal disorders. Clin Med (Lond) 2021;21:44-52.
3. Walker C, Boland A, Carroll A, et al. Concurrent functional gastrointestinal disorders in patients with inflammatory bowel disease. Frontiers in Gastroenterology 2022;Volume 1 - 2022.
4. Fagherazzi G, Gusto G, Balkau B, et al. Functional gastrointestinal disorders and incidence of type 2 diabetes: Evidence from the E3N–EPIC cohort study. Diabetes & Metabolism 2016;42:178-183.
5. Collier CA, Salikhova A, Sabir S, et al. Crisis in the gut: navigating gastrointestinal challenges in Gulf War Illness with bioengineering. Military Medical Research 2024;11:45.
6. Johnson AG, Hu Z, Cost AA. Incidence and recent trends in functional gastrointestinal disorders, active component, US Armed Forces, 2005-2014. MSMR 2016;23:10-15.
7. Margolis KG, Gershon MD, Bogunovic M. Cellular Organization of Neuroimmune Interactions in the Gastrointestinal Tract. Trends Immunol 2016;37:487-501.
8. Verheijden S, Boeckxstaens GE. Neuroimmune interaction and the regulation of intestinal immune homeostasis. Am J Physiol Gastrointest Liver Physiol 2018;314:G75-G80.
9. Wallrapp A, Chiu IM. Neuroimmune Interactions in the Intestine. Annu Rev Immunol 2024;42:489-519.
10. Kulkarni S, Kurapati S, Bogunovic M. Neuro-innate immune interactions in gut mucosal immunity. Curr Opin Immunol 2021;68:64-71.
11. Lakhan SE, Kirchgessner A. Neuroinflammation in inflammatory bowel disease. Journal of Neuroinflammation 2010;7:37.
12. Zhu Y, Meerschaert KA, Galvan-Pena S, et al. A chemogenetic screen reveals that Trpv1-expressing neurons control regulatory T cells in the gut. Science 2024;385:eadk1679.
13. Akiho H, Ihara E, Motomura Y, et al. Cytokine-induced alterations of gastrointestinal motility in gastrointestinal disorders. World J Gastrointest Pathophysiol 2011;2:72-81.
14. Kulkarni S, Micci MA, Leser J, et al. Adult enteric nervous system in health is maintained by a dynamic balance between neuronal apoptosis and neurogenesis. Proc Natl Acad Sci U S A 2017;114:E3709-E3718.
15. Wang H, Foong JPP, Harris NL, et al. Enteric neuroimmune interactions coordinate intestinal responses in health and disease. Mucosal Immunology 2022;15:27-39.

16. De Schepper S, Stakenborg N, Matteoli G, et al. Muscularis macrophages: Key players in intestinal homeostasis and disease. Cellular Immunology 2018;330:142-150.
17. Collier CA, Foncerrada S, Clevenger AJ, et al. Acute Exposure to Pyridostigmine Bromide Disrupts Cholinergic Myenteric Neuroimmune Function in Mice. Advanced Biology 2023;7:2200254.
18. Collier CA, Salikhova A, Sabir S, et al. Persistent enteric neuroinflammation chronically impairs colonic motility in a pyridostigmine bromide-induced mouse model of Gulf War Illness. Biology Open 2025.
19. Akiho H, Ihara E, Nakamura K. Low-grade inflammation plays a pivotal role in gastrointestinal dysfunction in irritable bowel syndrome. World J Gastrointest Pathophysiol 2010;1:97-105.
20. Spear ET, Mawe GM. Enteric neuroplasticity and dysmotility in inflammatory disease: key players and possible therapeutic targets. Am J Physiol Gastrointest Liver Physiol 2019;317:G853-g861.
21. Breßer M, Siemens KD, Schneider L, et al. Macrophage-induced enteric neurodegeneration leads to motility impairment during gut inflammation. EMBO Mol Med 2025;17:301-335.
22. Muller PA, Koscsó B, Rajani GM, et al. Crosstalk between muscularis macrophages and enteric neurons regulates gastrointestinal motility. Cell 2014;158:300-313.
23. Llorente C. The Imperative for Innovative Enteric Nervous System-Intestinal Organoid Co-Culture Models: Transforming GI Disease Modeling and Treatment. Cells 2024;13.
24. Collier CA, Mendiondo C, Raghavan S. Tissue engineering of the gastrointestinal tract: the historic path to translation. Journal of Biological Engineering 2022;16.
25. Hibiya S, Tsuchiya K, Hayashi R, et al. Long-term Inflammation Transforms Intestinal Epithelial Cells of Colonic Organoids. J Crohns Colitis 2017;11:621-630.
26. Zhang Z, Engel MA, Koch E, et al. Menthacarin induces calcium ion influx in sensory neurons, macrophages and colonic organoids of mice. Life Sci 2021;264:118682.
27. Flood P, Hanrahan N, Nally K, et al. Human intestinal organoids: Modeling gastrointestinal physiology and immunopathology — current applications and limitations. European Journal of Immunology 2024;54:2250248.
28. Liebregts T, Adam B, Bredack C, et al. Immune activation in patients with irritable bowel syndrome. Gastroenterology 2007;132:913-920.
29. Billiet T, Paul R, Marc F, et al. Targeting TNF-α for the treatment of inflammatory bowel disease. Expert Opinion on Biological Therapy 2014;14:75-101.
30. Huycke TR, Miller BM, Gill HK, et al. Genetic and Mechanical Regulation of Intestinal Smooth Muscle Development. Cell 2019;179:90-105.e21.
31. Sharkey KA, Mawe GM. The enteric nervous system. Physiological Reviews 2023;103:1487-1564.
32. Kigata T, Koyama T, Lu X, et al. Quantitative analysis of the distribution of the myenteric plexus in the rabbit large intestine. Anatomia, Histologia, Embryologia 2023;52:1029-1033.
33. Furness JB. Types of neurons in the enteric nervous system. Journal of the Autonomic Nervous System 2000;81:87-96.
34. Heanue TA, Pachnis V. Prospective Identification and Isolation of Enteric Nervous System Progenitors Using Sox2. Stem Cells 2011;29:128-140.
35. Metzger M, Bareiss PM, Danker T, et al. Expansion and Differentiation of Neural Progenitors Derived From the Human Adult Enteric Nervous System. Gastroenterology 2009;137:2063-2073.e4.
36. Belkind-Gerson J, Hotta R, Nagy N, et al. Colitis Induces Enteric Neurogenesis Through a 5-HT4–dependent Mechanism. Inflammatory Bowel Diseases 2015;21:870-878.

37. Belkind-Gerson J, Graham HK, Reynolds J, et al. Colitis promotes neuronal differentiation of Sox2+ and PLP1+ enteric cells. Scientific reports 2017;7:2525.
38. Nair DG, Miller KG, Lourenssen SR, et al. Inflammatory cytokines promote growth of intestinal smooth muscle cells by induced expression of PDGF-Rβ. Journal of Cellular and Molecular Medicine 2014;18:444-454.
39. Alkahtani R, Mahavadi S, Al-Shboul O, et al. Changes in the expression of smooth muscle contractile proteins in TNBS- and DSS-induced colitis in mice. Inflammation 2013;36:1304-15.
40. Khaiboullina SF, DeMeirleir KL, Rawat S, et al. Cytokine expression provides clues to the pathophysiology of Gulf War illness and myalgic encephalomyelitis. Cytokine 2015;72:1-8.
41. Kalahasty K, Lee Y, Locatelli E, et al. Ocular and inflammatory markers associated with Gulf War illness symptoms. Scientific Reports 2023;13:3512.
42. Trageser KJ, Sebastian-Valverde M, Naughton SX, et al. The Innate Immune System and Inflammatory Priming: Potential Mechanistic Factors in Mood Disorders and Gulf War Illness. Frontiers in Psychiatry 2020;Volume 11 - 2020.
43. Souza RF, Caetano MAF, Magalhães HIR, et al. Study of tumor necrosis factor receptor in the inflammatory bowel disease. World J Gastroenterol 2023;29:2733-2746.
44. Vulliemoz M, Brand S, Juillerat P, et al. TNF-Alpha Blockers in Inflammatory Bowel Diseases: Practical Recommendations and a User's Guide: An Update. Digestion 2020;101:16-26.
45. Speca S, Giusti I, Rieder F, et al. Cellular and molecular mechanisms of intestinal fibrosis. World J Gastroenterol 2012;18:3635-61.
46. Au-Yeung N, Mandhana R, Horvath CM. Transcriptional regulation by STAT1 and STAT2 in the interferon JAK-STAT pathway. JAK-STAT 2013;2:e23931.
47. Sharma BR, Karki R, Sundaram B, et al. The Transcription Factor IRF9 Promotes Colorectal Cancer via Modulating the IL-6/STAT3 Signaling Axis. Cancers (Basel) 2022;14.
48. Roy S, Guler R, Parihar SP, et al. Batf2/Irf1 Induces Inflammatory Responses in Classically Activated Macrophages, Lipopolysaccharides, and Mycobacterial Infection. The Journal of Immunology 2015;194:6035-6044.
49. Hardaker EL, Bacon AM, Carlson K, et al. Regulation of TNF-α and IFN-γ induced CXCL10 expression: participation of the airway smooth muscle in the pulmonary inflammatory response in chronic obstructive pulmonary disease. The FASEB Journal 2004;18:191-193.
50. Elia G, Guglielmi G. CXCL9 chemokine in ulcerative colitis. La Clinica Terapeutica 2018;169:e235-e241.
51. Nagasubramanian K, Gupta K. Interactome analysis implicates class II transactivator (CIITA) in depression and other neuroinflammatory disorders. International Journal of Neuroscience 2024;134:1153-1171.
52. Grabacka M, Płonka PM, Pierzchalska M. The PPARα regulation of the gut physiology in regard to interaction with microbiota, intestinal immunity, metabolism, and permeability. International Journal of Molecular Sciences 2022;23:14156.
53. Meng EX, Verne GN, Zhou Q. Macrophages and Gut Barrier Function: Guardians of Gastrointestinal Health in Post-Inflammatory and Post-Infection Responses. Int J Mol Sci 2024;25.
54. Luo J, Lian Q, Zhu D, et al. PLSCR1 promotes apoptosis and clearance of retinal ganglion cells in glaucoma pathogenesis. Genes & Diseases 2023;10:1564-1581.
55. Mockenhaupt K, Gonsiewski A, Kordula T. RelB and Neuroinflammation. Cells 2021;10:1609.

56. Ormestad M, Astorga J, Landgren H, et al. Foxf1 and Foxf2 control murine gut development by limiting mesenchymal Wnt signaling and promoting extracellular matrix production. Development 2006;133:833-843.
57. Kofla-Dlubacz A, Matusiewicz M, Krzystek-Korpacka M, et al. Correlation of MMP-3 and MMP-9 with Crohn's disease activity in children. Dig Dis Sci 2012;57:706-12.
58. Yamashita A, Inamine T, Suzuki S, et al. Genetic variants of SMAD2/3/4/7 are associated with susceptibility to ulcerative colitis in a Japanese genetic background. Immunology Letters 2019;207:64-72.
59. Jaeger N, Gamini R, Cella M, et al. Single-cell analyses of Crohn's disease tissues reveal intestinal intraepithelial T cells heterogeneity and altered subset distributions. Nature Communications 2021;12:1921.
60. Popivanova BK, Kostadinova FI, Furuichi K, et al. Blockade of a Chemokine, CCL2, Reduces Chronic Colitis-Associated Carcinogenesis in Mice. Cancer Research 2009;69:7884-7892.
61. Leal RF, Planell N, Kajekar R, et al. Identification of inflammatory mediators in patients with Crohn's disease unresponsive to anti-TNFα therapy. Gut 2015;64:233-242.
62. Tagore A, Gonsalkorale W, Pravica V, et al. Interleukin-10 (IL-10) genotypes in inflammatory bowel disease. Tissue antigens 1999;54:386-390.
63. Polosukhina D, Singh K, Asim M, et al. CCL11 exacerbates colitis and inflammation-associated colon tumorigenesis. Oncogene 2021;40:6540-6546.
64. Mudter J, Neurath MF. Il-6 signaling in inflammatory bowel disease: pathophysiological role and clinical relevance. Inflammatory bowel diseases 2007;13:1016-1023.
65. Woolf CJ, Safieh-Garabedian B, Ma QP, et al. Nerve growth factor contributes to the generation of inflammatory sensory hypersensitivity. Neuroscience 1994;62:327-31.
66. Rai MF, Cai L, Chinzei N, et al. Distinct patterns of cytokines, chemokines, and growth factors in synovial fluid after ACL injury in comparison to osteoarthritis. Journal of Orthopaedic Research 2024;42:1448-1462.
67. Kapsoritakis AN, Kapsoritaki AI, Davidi IP, et al. Imbalance of tissue inhibitors of metalloproteinases (TIMP) – 1 and – 4 serum levels, in patients with inflammatory bowel disease. BMC Gastroenterology 2008;8:55.
68. Mimura T, Bateman AC, Lee RL, et al. Up-regulation of collagen and tissue inhibitors of matrix metalloproteinase in colonic diverticular disease. Dis Colon Rectum 2004;47:371-8; discussion 378-9.
69. Polosukhina D, Singh K, Asim M, et al. CCL11 exacerbates colitis and inflammation-associated colon tumorigenesis. Oncogene 2021;40:6540-6546.
70. Whistler T, Fletcher MA, Lonergan W, et al. Impaired immune function in Gulf War Illness. BMC Medical Genomics 2009;2:12.
71. Longange B. Defining the Neurochemical Phenotype of Myenteric Neurons that Display Nerve Growth Factor Promotor Activity in Adult Transgenic Mice - Implications for Colonic Inflammation. Canada -- Ontario, CA: Queen's University (Canada), 2022:66.
72. Shi X-Z, Winston JH, Sarna SK. Differential immune and genetic responses in rat models of Crohn's colitis and ulcerative colitis. American Journal of Physiology-Gastrointestinal and Liver Physiology 2011;300:G41-G51.
73. Vrees MD, Pricolo VE, Potenti FM, et al. Abnormal Motility in Patients With Ulcerative Colitis: The Role of Inflammatory Cytokines. Archives of Surgery 2002;137:439-446.
74. Winston JH, Li Q, Sarna SK. Paradoxical regulation of ChAT and nNOS expression in animal models of Crohn's colitis and ulcerative colitis. American Journal of Physiology-Gastrointestinal and Liver Physiology 2013;305:G295-G302.
75. Becker L, Nguyen L, Gill J, et al. Age-dependent shift in macrophage polarisation causes inflammation-mediated degeneration of enteric nervous system. Gut 2018;67:827-836.

76. Candiotti K. A primer on nerve agents: what the emergency responder, anesthesiologist, and intensivist needs to know. Can J Anaesth 2017;64:1059-1070.
77. Grundmann D, Loris E, Maas-Omlor S, et al. Enteric Neurogenesis During Life Span Under Physiological and Pathophysiological Conditions. Anat Rec (Hoboken) 2019;302:1345-1353.
78. Souza RF, Machado FA, Caetano MAF, et al. Effect of Anti-TNF Monoclonal Antibody on Enteric Neurons and Enteric Glial Cells in Experimental Colitis. Dig Dis Sci 2025;70:1375-1394.
79. Gougeon PY, Lourenssen S, Han TY, et al. The pro-inflammatory cytokines IL-1beta and TNFalpha are neurotrophic for enteric neurons. J Neurosci 2013;33:3339-51.
80. Veisman I, Massey WJ, Goren I, et al. Muscular hyperplasia in Crohn's disease strictures: through thick and thin. American Journal of Physiology-Cell Physiology 2024;327:C671-C683.
81. Chen W, Lu C, Hirota C, et al. Smooth muscle hyperplasia/hypertrophy is the most prominent histological change in Crohn's fibrostenosing bowel strictures: a semiquantitative analysis by using a novel histological grading scheme. Journal of Crohn's and Colitis 2017;11:92-104.
82. Wang WF, Guo XX, Yang YS. Gastrointestinal problems in modern wars: clinical features and possible mechanisms. Mil Med Res 2015;2:15.
83. Bassotti G, Antonelli E, Villanacci V, et al. Colonic motility in ulcerative colitis. United European Gastroenterol J 2014;2:457-62.
84. da Silva Watanabe P, Cavichioli AM, de Lima Mendes JDA, et al. Colonic motility adjustments in acute and chronic DSS-induced colitis. Life Sciences 2023;321:121642.
85. Ansari R, Attari F, Razjouyan H, et al. Ulcerative colitis and irritable bowel syndrome: relationships with quality of life. European journal of gastroenterology & hepatology 2008;20:46-50.
86. Piche T, Ducrotté P, Sabate J, et al. Impact of functional bowel symptoms on quality of life and fatigue in quiescent Crohn disease and irritable bowel syndrome. Neurogastroenterology & Motility 2010;22:626-e174.
87. Trivedi KH, Schlett CD, Tribble DR, et al. The impact of post-infectious functional gastrointestinal disorders and symptoms on the health-related quality of life of US military personnel returning from deployment to the Middle East. Digestive diseases and sciences 2011;56:3602-3609.
88. Raghavan S, Gilmont RR, Miyasaka EA, et al. Successful implantation of bioengineered, intrinsically innervated, human internal anal sphincter. Gastroenterology 2011;141:310-9.
89. Li S, Fei G, Fang X, et al. Changes in Enteric Neurons of Small Intestine in a Rat Model of Irritable Bowel Syndrome with Diarrhea. J Neurogastroenterol Motil 2016;22:310-20.
90. Takahashi T. Pathophysiological significance of neuronal nitric oxide synthase in the gastrointestinal tract. J Gastroenterol 2003;38:421-30.
91. Wells R, Blennerhassett M. Persistent and selective effects of inflammation on smooth muscle cell contractility in rat colitis. Pflügers Archiv 2004;448:515-524.
92. MacDonald J. Smooth muscle phenotypic plasticity in mechanical obstruction of the small intestine. Neurogastroenterology & Motility 2008;20:737-740.
93. Anitha M, Joseph I, Ding X, et al. Characterization of fetal and postnatal enteric neuronal cell lines with improvement in intestinal neural function. Gastroenterology 2008;134:1424-1435.
94. Spera I, Sánchez-Rodríguez R, Favia M, et al. The J2-Immortalized Murine Macrophage Cell Line Displays Phenotypical and Metabolic Features of Primary BMDMs in Their M1 and M2 Polarization State. Cancers (Basel) 2021;13.

95. Balasubramaniam A, Li G, Ramanathan A, et al. SIRT3 activation promotes enteric neurons survival and differentiation. Scientific reports 2022;12:22076.
96. Bankhead P. Analyzing fluorescence microscopy images with ImageJ, 2014.
97. Clevenger AJ, McFarlin MK, Collier CA, et al. Peristalsis-Associated Mechanotransduction Drives Malignant Progression of Colorectal Cancer. Cellular and Molecular Bioengineering 2023;16:261-281.
98. Keenan AB, Torre D, Lachmann A, et al. ChEA3: transcription factor enrichment analysis by orthogonal omics integration. Nucleic Acids Res 2019;47:W212-w224.
99. Zhou G, Soufan O, Ewald J, et al. NetworkAnalyst 3.0: a visual analytics platform for comprehensive gene expression profiling and meta-analysis. Nucleic Acids Research 2019;47:W234-W241.
100. Metzger M, Bareiss PM, Danker T, et al. Expansion and differentiation of neural progenitors derived from the human adult enteric nervous system. Gastroenterology 2009;137:2063-2073. e4.